

Supporting Information for

Examining the role of Rh/Si cooperation in alkene hydrogenation by a pincer-type [P₂Si]Rh complex

Matthew T. Whited,*^a Alexander M. Deetz,[†] Theodore M. Donnell,[†] and Daron E. Janzen[‡]

[†] Department of Chemistry, Carleton College, Northfield, MN 55057, United States

[‡] Department of Chemistry and Biochemistry, St. Catherine University, St. Paul, MN 55105, United States

Experimental Section	S2
General Considerations.....	S2
[(^{Ph} P ₂ Si)RhOTf] ₂ (^{Ph} 2)	S3
^{Cy} P ₂ SiH ₂ ligand	S3
[^{Cy} P ₂ SiOTf]Rh(nbd) (^{Cy} 1-OTf}).....	S4
[^{Cy} P ₂ SiMe]Rh(nbd) (^{Cy} 1-Me})	S5
[^{Cy} P ₂ SiH]Rh(H)(OTf) (^{Cy} 3-H}).....	S6
[^{Cy} P ₂ SiMe]Rh(H)(OTf) (^{Cy} 3-Me}).....	S7
Catalytic Hydrogenation of Norbornene and Monitoring by GC-MS.....	S7
Figure S1. Comparison of Catalyst Activities for Norbornene Hydrogenation.....	S9
Hydrogenation of Norbornene under H ₂ /D ₂	S9
Figure S2. Partial mass spectrum for norbornane-d ₀	S10
Figure S3. Partial mass spectrum for norbornane-d ₂	S10
Figure S4. Partial mass spectrum for mixture of norbornane-d ₀ , -d ₁ , and -d ₂ obtained from hydrogenation of norbornene by ^{Cy} 1-OTf	S10
Computational Details.	S11
Figure S5. DFT minimized structure of ^{Me} 3-H	S12
XYZ Coordinates for ^{Me} 3-H	S13
Figure S6. DFT minimized structure of ^{Me} 4-OTf	S14
XYZ Coordinates for ^{Me} 4-OTf	S15
X-ray Crystallography.....	S16
Special Crystallographic Refinement Details.	S17
Figure S7. Crystal structure of ^{Cy} P ₂ SiH ₂	S17
Table S1. X-ray crystallographic data	S18
Figure S8. ¹ H NMR spectrum of ^{Cy} P ₂ SiH ₂ in CDCl ₃	S19
Figure S9. ¹³ C NMR spectrum of ^{Cy} P ₂ SiH ₂ in CDCl ₃	S20
Figure S10. ²⁹ Si NMR spectrum of ^{Cy} P ₂ SiH ₂ in CDCl ₃	S21
Figure S11. ³¹ P NMR spectrum of ^{Cy} P ₂ SiH ₂ in CDCl ₃	S22
Figure S12. ¹ H NMR spectrum of [^{Cy} P ₂ SiOTf]Rh(nbd) (^{Cy} 1-OTf}) in C₆D₆	S23
Figure S13. ¹³ C NMR spectrum of [^{Cy} P ₂ SiOTf]Rh(nbd) (^{Cy} 1-OTf}) in C₆D₆	S24
Figure S14. ¹⁹ F NMR spectrum of [^{Cy} P ₂ SiOTf]Rh(nbd) (^{Cy} 1-OTf}) in C₆D₆.....	S25
Figure S15. ²⁹ Si NMR spectrum of [^{Cy} P ₂ SiOTf]Rh(nbd) (^{Cy} 1-OTf}) in C₆D₆.....	S26
Figure S16. ³¹ P NMR spectrum of [^{Cy} P ₂ SiOTf]Rh(nbd) (^{Cy} 1-OTf}) in C₆D₆	S27
Figure S17. ²⁹ Si NMR spectrum of [^{Cy} P ₂ SiOTf]Rh(nbd) (^{Cy} 1-OTf}) in C₆D₆ after partial decomposition.....	S28
Figure S18. ³¹ P NMR spectrum of [^{Cy} P ₂ SiOTf]Rh(nbd) (^{Cy} 1-OTf}) in C₆D₆ after partial decomposition.....	S29
Figure S19. ¹ H NMR spectrum of [^{Cy} P ₂ SiMe]Rh(nbd) (^{Cy} 1-Me}) in C₆D₆	S30
Figure S20. ¹³ C NMR spectrum of [^{Cy} P ₂ SiMe]Rh(nbd) (^{Cy} 1-Me}) in C₆D₆	S31
Figure S21. ²⁹ Si NMR spectrum of [^{Cy} P ₂ SiMe]Rh(nbd) (^{Cy} 1-Me}) in C₆D₆	S32

Figure S22. ^{31}P NMR spectrum of $[\text{CyP}_2\text{Si}^{\text{Me}}]\text{Rh}(\text{nbd})$ (Cy1-Me) in C_6D_6	S33
Figure S23. ^1H NMR spectrum of $[\text{CyP}_2\text{Si}^{\text{H}}]\text{Rh}(\text{nbd})$ (Cy3-H) in C_6D_6	S34
Figure S24. ^{19}F NMR spectrum of $[\text{CyP}_2\text{Si}^{\text{H}}]\text{Rh}(\text{nbd})$ (Cy3-H) in C_6D_6	S35
Figure S25. $^1\text{H}/^{29}\text{Si}$ HMQC NMR spectrum of $[\text{CyP}_2\text{Si}^{\text{H}}]\text{Rh}(\text{nbd})$ (Cy3-H) in C_6D_6	S36
Figure S26. ^{31}P NMR spectrum of $[\text{CyP}_2\text{Si}^{\text{H}}]\text{Rh}(\text{nbd})$ (Cy3-H) in C_6D_6	S37
Figure S27. ^1H NMR spectrum of $[\text{CyP}_2\text{Si}^{\text{Me}}]\text{Rh}(\text{H})(\text{OTf})$ (Cy3-Me) in C_6D_6	S38
Figure S28. ^{13}C NMR spectrum of $[\text{CyP}_2\text{Si}^{\text{Me}}]\text{Rh}(\text{H})(\text{OTf})$ (Cy3-Me) in C_6D_6	S39
Figure S29. ^{19}F NMR spectrum of $[\text{CyP}_2\text{Si}^{\text{Me}}]\text{Rh}(\text{H})(\text{OTf})$ (Cy3-Me) in C_6D_6	S40
Figure S30. ^{29}Si NMR spectrum of $[\text{CyP}_2\text{Si}^{\text{Me}}]\text{Rh}(\text{H})(\text{OTf})$ (Cy3-Me) in C_6D_6	S41
Figure S31. ^{31}P NMR spectrum of $[\text{CyP}_2\text{Si}^{\text{Me}}]\text{Rh}(\text{H})(\text{OTf})$ (Cy3-Me) in C_6D_6	S42
References	S43

Experimental Section

General Considerations. All manipulations were carried out under a dinitrogen atmosphere in an MBraun Unilab 2000 glove box or under an argon atmosphere using standard Schlenk techniques. Routine solvents were purchased from Aldrich and were deoxygenated and dried using a Glass Contour Solvent Purification System, except for anhydrous benzene and pentane, which were used as received from Aldrich. Tetraethylorthosilicate was used as received from Strem. Bis(norbornadiene)rhodium(I) triflate, silver(I) triflate, and lithium aluminum hydride were used as received from Aldrich. *tert*-Butyllithium was purchased from Aldrich as a 1.5-M solution in pentane, isolated as a solid by removal of volatile components *in vacuo*, and stored in the dark at -35°C . $(2\text{-bromophenyl})\text{dicyclohexylphosphine}$,¹ ($^{\text{Ph}}\text{P}_2\text{Si}^{\text{OTf}}$) $\text{Rh}(\text{nbd})$ (**Ph1-OTf**),² and $[\text{CyP}_2\text{Si}^{\text{Me}}]\text{Rh}(\text{H})(\text{Cl})$ ³ were prepared according to published methods. NMR solvents (Cambridge Isotope Labs) were degassed and passed through a pad of activated alumina prior to use. Alumina was activated by heating at 300°C for 8–12 h under vacuum prior to use. NMR spectra were recorded at ambient temperature on a Bruker Avance III HD 400 High Performance Digital NMR spectrometer. ^1H and ^{13}C NMR chemical shifts were referenced to residual solvent, ^{19}F , ^{29}Si , and ^{31}P NMR chemical shifts are reported relative to external standards of hexafluorobenzene ($\delta = -163$),

85% H₃PO₄, and tetramethylsilane, respectively. Microanalysis was carried out by Midwest Microlab, LLC.

[(^{Ph}P₂Si)RhOTf]₂ (^{Ph}2). In a typical preparation, a saturated dichloromethane solution of [^{Ph}P₂SiOTf]Rh(nbd) (**Ph1-OTf**, 10 mg, prepared as previously described²) was subjected to vapor cross diffusion with pentane at –35 °C for 3 d, leading to a small crop of red prisms identified as **Ph2** by X-ray crystallography. **Ph2** proved insoluble in common glove box solvents (e.g., tetrahydrofuran, dichloromethane, and toluene) and was only obtained in low yields, frequently co-crystallizing with yellow **Ph1-OTf**, precluding satisfactory bulk analysis.

^{Cy}P₂SiH₂ ligand. This ligand was prepared according to our previously reported method for the phenyl derivative.² In an inert atmosphere glovebox, (2-bromophenyl)dicyclohexylphosphine (1.06 g, 2.98 mmol) was dissolved in diethyl ether (ca. 40 mL) in a 100-mL pressure tube. The reaction flask was attached to an argon manifold and cooled to –78 °C. *tert*-Butyllithium (380 mg, 5.93 mmol) dissolved in pentane (ca. 10 mL) was added dropwise via syringe to the reaction flask, which was allowed to warm to ambient temperature over 2 h. Tetraethylorthosilicate (330 μL, 1.48 mmol) dissolved in diethyl ether (ca. 5 mL) was added dropwise via syringe to the reaction mixture and allowed to stir overnight. The vessel was returned to the glovebox and lithium aluminum hydride (140 mg, 3.0 mmol) in diethyl ether (10 mL) was added and the mixture allowed to stir for 5 h. The solution was filtered through a 2-cm silica plug, which was washed with additional diethyl ether, and the filtrate was dried *in vacuo* to afford (^{Cy}P₂Si)H₂ as a white powder. Yield: 642 mg, 75%. Colorless crystals of ^{Cy}P₂SiH₂ suitable for X-ray diffraction were obtained from a concentrated diethyl ether solution by vapor cross diffusion with pentane at –35 °C. ¹H

¹H NMR (400 MHz, CDCl₃): δ 7.60 (dt, Ar–H *ortho* to Si, *J* = 7.4, 1.8 Hz, 2H), 7.47 (br d, Ar–H, *J* = 7.9 Hz, 2H), 7.35 (td, Ar–H, *J* = 7.5, 1.5 Hz, 2H), 7.26 (tt, Ar–H, *J* = 7.9, 1.3 Hz, 2H), 5.40 (t, Si–H, ⁴J_{HP} = 9.2 Hz, 2H), 1.90–1.80 (m, 8H), 1.77–1.67 (m, 4H), 1.62–1.52 (m, 8H), 1.50–1.42 (m, 4H), 1.30–1.05 (m, 16H), 1.00–0.90 (m, 4H). ¹³C NMR (101 MHz, CDCl₃): δ 143.8 (dd, *J* = 47, 5 Hz), 143.4 (d, *J* = 15 Hz), 138.4 (dd, *J* = 15, 3 Hz), 132.0 (d, *J* = 2 Hz), 129.0, 128.0–127.8 (d, *J* = 1 Hz), 34.9 (d, *J* = 14 Hz), 30.5 (d, *J* = 16 Hz), 29.6 (d, *J* = 9 Hz), 27.3 (d, *J* = 3 Hz), 27.23, 26.59. ²⁹Si{¹H} NMR (79 MHz, CDCl₃): δ –40.0 (t, ³J_{SiP} = 22 Hz). ³¹P{¹H} NMR (162 MHz, CDCl₃): δ –5.8 (s).

[^{Cy}P₂SiOTf]Rh(nbd) (^{Cy}1-OTf). A solution of ^{Cy}P₂SiH₂ (56.7 mg, 0.0983 mmol) in CH₂Cl₂ (2 mL) was added dropwise to a stirring solution of [Rh(nbd)₂]OTf (42.9 mg, 0.0983 mmol) in CH₂Cl₂ (ca. 3 mL) at –35 °C. Toluene (5 mL) was immediately added to the mixture and all solvent was removed *in vacuo*. The resulting film was redissolved in benzene (3 mL), frozen at –35 °C, and lyophilized to afford ^{Cy}1-OTf as a flocculent yellow powder. Yield: 82.3 mg, 91%. Crystals suitable for X-ray diffraction were obtained by chilling a saturated diethyl ether solution of ^{Cy}1-OTf at –35 °C. ¹H NMR (400 MHz, C₆D₆): δ 8.36 (d, *J* = 6.9 Hz, 2H, Ar–H *ortho* to Si), 7.48 (d, *J* = 7.5 Hz, 2H), 7.16 (apparent t, *J* = 7.4 Hz, 2H), 7.08 (apparent t, *J* = 7.4 Hz, 2H), 5.24 (br, 2H), 3.73 (br, 2H), 3.46 (br, 2H), 2.68 (t, *J* = 11.8 Hz, 2H), 2.29 (d, *J* = 13.2 Hz, 2H), 2.19 (br, 2H), 1.94–0.96 (m, 40H). ¹³C: 153.1–152.3 (m), 145.6–145.1 (m), 132.8 (t, *J* = 10 Hz), 129.8, 128.8 (br), 119.7 (q, ¹J_{FC} = 318 Hz, –CF₃), 74.9 (dd, *J* = 5.4, 2.6 Hz), 64.6 (dd, *J* = 6.1, 3.1 Hz), 48.1, 43.2 (t, *J* = 10.9 Hz), 38.0 (t, *J* = 3.6 Hz), 37.0–36.7 (m), 31.0, 30.5 (br), 29.2, 28.4 (t, *J* = 4.2 Hz), 28.1 (t, *J* = 5.6 Hz), 27.5–27.2 (m), 27.1, 26.3. ¹⁹F{¹H} NMR (376 MHz, C₆D₆): δ –76.8. ²⁹Si{¹H} NMR (80 MHz, C₆D₆): δ 92.2 (dt, ¹J_{RhSi} = 49 Hz, ²J_{PSi} = 18 Hz). ³¹P{¹H} NMR (162

MHz, C₆D₆): δ 57.0 (d, ¹J_{RhP} = 138 Hz). Anal. calcd. for C₄₄H₆₀F₃O₃P₂RhSiS: C, 57.51; H, 6.58. Found: C, 57.53; H, 6.54. **NOTE:** ^{Cy}**1-OTf** was unstable in solution over extended periods, so NMR spectra requiring substantial time to collect (¹³C and ²⁹Si) contain evidence of an as-yet-unidentified decomposition product with distinct phosphine environments and extremely large P–P coupling constants. Key spectral data for decomposition product from ^{Cy}**1-OTf**: ²⁹Si{¹H} NMR (80 MHz, C₆D₆): δ 65.2 (ddd, *J* = 39.5, 7.2, 4.5 Hz); ³¹P NMR (162 MHz, C₆D₆): δ 51.8 (dd, ¹J_{RhP} = 146 Hz, *J*_{PP} = 313 Hz), 30.9 (dd, ¹J_{RhP} = 130 Hz, *J*_{PP} = 313 Hz).

[^{Cy}P₂Si^{Me}]Rh(nbd) (Cy1-Me**).** To a stirring solution of [^{Cy}P₂Si^{Me}]Rh(H)(Cl) (30.0 mg, 0.0411 mmol) in tetrahydrofuran (5 mL) at –35 °C was added a solution of lithium triethylborohydride (41 μL, 1.0 M in THF, 0.041 mmol) dropwise. The reaction was allowed to proceed for 1 h. Volatile components were removed *in vacuo* to afford a light brown powder, and pure Cy**1-Me** was obtained as a brown semicrystalline solid from a concentrated pentane solution by slow evaporation into HMDSO at –35 °C. Yield: 8.7 mg, 27%. ¹H NMR (400 MHz, C₆D₆): δ 7.59 (dd, *J* = 7.2, 2.1 Hz, 2H), 7.75 (br d, *J* = 7.0 Hz, 2H), 7.16–7.08 (m, 4H), 5.32 (s, 2H), 3.55 (br, 2H), 3.05 (br, 2H), 2.61 (br, 2H), 2.24 (br, 2H), 2.08 (m, 2H), 1.93 (d, *J* = 12.9 Hz, 2H), 1.86–1.54 (m, 18H), 1.46 (m, 8H), 1.32–1.07 (m, 14H), 0.51 (s, 3H, Si–CH₃). ¹³C{¹H} NMR (101 MHz, C₆D₆): δ 159.0–157.9 (m), 146.5–146.0 (m), 132.2 (t, *J* = 11.1 Hz), 128.6, 127.2, 77.2, 63.4, 48.1, 42.8 (t, *J* = 10.3 Hz), 39.5 (m), 31.6–31.2 (m), 31.0, 30.6 (m), 30.3, 29.3, 28.4–28.0 (m), 27.8 (t, *J* = 4.4 Hz), 27.2, 26.7, –2.4. ²⁹Si{¹H} NMR (80 MHz, C₆D₆): δ 53.1 (dt, ¹J_{RhSi} = 34.4 Hz, ²J_{PSi} = 12.1 Hz). ³¹P{¹H} NMR (162 MHz, C₆D₆): δ 58.7 (d, ¹J_{RhP} = 142.2 Hz).

[^{Cy}P₂Si^H]Rh(H)(OTf) (^{Cy}3-H). A solution of ^{Cy}1-OTf (ca. 10 mg) in 700 μ L diethyl ether was transferred to a J Young tube and the headspace evacuated by one freeze–pump–thaw cycle and backfilled with H₂ (0.5 atm). The reaction was monitored by ³¹P NMR spectroscopy, and volatiles were removed *in vacuo* as soon as conversion to ^{Cy}3-H was complete (ca. 30 min), affording ^{Cy}3-H in 90–95% purity, as judged by ¹H, ¹⁹F, and ³¹P NMR spectroscopy. The complex was unstable for extended periods in all solvents examined, and decomposition was particularly rapid under H₂, precluding further spectroscopic characterization. ¹H NMR (400 MHz, C₆D₆): δ 7.94 (d, J = 7.3 Hz, 2H), 7.29–7.24 (m, 2H), 7.20–7.15 (m, 2H), 7.09 (t, J = 7.5 Hz, 2H), 5.65 (s, 1H, Si–H; ²⁹Si satellites show $^1J_{\text{SiH}}$ = 117 Hz), 2.95 (t, J = 12.1 Hz, 2H), 2.58–2.09 (m, 10H), 1.91–1.76 (m, 4H), 1.65–1.05 (m, 26H), 0.82–0.65 (m, 4H), –22.62 (dtd, $^1J_{\text{RhH}}$ = 31.5 Hz, $^2J_{\text{PH}}$ = 13.4 Hz, $^3J_{\text{HH(Si)}}$ = 4.4 Hz, 1H, Rh–H). ¹⁹F NMR (376 MHz, C₆D₆) δ –76.8. ²⁹Si NMR (80 MHz, C₆D₆, determined by ¹H/²⁹Si HMBC): δ 26.6 ($^1J_{\text{SiH}}$ = 195 Hz). ³¹P (162 MHz, C₆D₆): δ 60.4 (dd, $^1J_{\text{RhP}}$ = 117 Hz, $^2J_{\text{PH(hydride)}}$ = 13 Hz).

[^{Cy}P₂Si^{Me}]Rh(H)(OTf) (^{Cy}3-Me). To a solution of [^{Cy}P₂Si^{Me}]Rh(H)(Cl) (18.5 mg, 0.0254 mmol) in diethyl ether (3 mL) was added a solution of silver triflate (926 μ L, 0.027 M in Et₂O, 0.025 mmol) with stirring. A precipitate formed immediately as the solution lightened slightly. After 1 h, the solution was filtered and volatiles removed *in vacuo* to afford a yellow powder that was redissolved in benzene (ca. 3 mL), filtered, and lyophilized to give pure ^{Cy}3-Me. Yield: 15.4 mg, 72%. Nearly colorless polycrystalline product was obtained from a concentrated pentane solution of ^{Cy}3-Me by slow evaporation into HMDSO at –35 °C. ¹H NMR (400 MHz, C₆D₆): δ 7.87 (d, J = 7.3 Hz, 2H), 7.34–7.28 (m, 2H), 7.20 (td, J = 7.3, 1.0 Hz, 2H), 7.10 (td, J = 7.5, 1.3 Hz), 2.92 (t, J = 11.4 Hz, 2H), 2.50 (d, J = 12.3 Hz, 2H), 2.45–2.28 (m, 4H), 2.14–2.00 (m, 2H),

1.92 (m, 2H), 1.82 (m, 2H), 1.71–1.59 (m, 8H), 1.51 (d, J = 13.1 Hz, 4H), 1.43–1.04 (m, 14H), 0.91 (s, 3H, Si–CH₃), 0.89–0.74 (m, 4H), –22.43 (dt, $^1J_{\text{RhH}}$ = 32.1 Hz, $^2J_{\text{PH}}$ = 13.8 Hz, 1H, Rh–H). ^{13}C NMR (101 MHz, C₆D₆): δ 156.3 (t, J = 21 Hz), 139.8 (t, J = 23 Hz), 132.2 (t, J = 10 Hz), 131.0, 129.8, 34.8 (t, J = 13 Hz), 34.3 (t, J = 9 Hz), 30.9, 30.0, 29.6, 27.7, 27.5–26.9 (m), 26.4, 6.9 [NOTE: The triflate –CF₃ was not observed by ^{13}C NMR]. ^{19}F NMR (376 MHz, C₆D₆): δ 76.4. ^{29}Si NMR (80 MHz, C₆D₆): δ 47.9 (apparent dq, $^1J_{\text{RhSi}}$ = 36 Hz, $^2J_{\text{PSi}} \approx ^2J_{\text{SiH(hydride)}}$ = 3 Hz). ^{31}P NMR (162 MHz, C₆D₆): δ 59.5 (dd, $^1J_{\text{RhP}}$ = 120 Hz, $^2J_{\text{PH}}$ = 13 Hz).

Catalytic Hydrogenation of Norbornene and Monitoring by GC-MS. A solution of norbornene (77 mM) and the appropriate [P₂Si] rhodium precatalyst (**Cy1-OTf**, **Cy1-Me**, or **Cy3-Me**; 0.38 mM) in 5.0 mL diethyl ether was transferred to a pressure tube with a stir bar in an inert atmosphere glove box. On a Schlenk line, the mixture was subjected to one freeze–pump–thaw cycle and allowed to warm to ambient temperature under static vacuum. The headspace was backfilled and purged (ca. 30 sec) with hydrogen while the mixture was stirred at 1100 RPM, and the valve for the reaction vessel was replaced with a septum. The reaction was allowed to proceed under H₂ (1 atm) with stirring, and aliquots were removed by cannula at regular intervals. Each aliquot was immediately filtered through a plug of activated alumina into a GC-MS vial for analysis. The norbornane:norbornene ratio was calculated by applying a previously determined relative response factor to integrated signals for the parent ion peaks at *m/z* 94.1 (norbornene) and 96.1 (norbornane) (i.e., the integrated area for the norbornane parent peak was multiplied by 1.8 to account for its relatively lower response compared with norbornene). Comparisons of catalyst activities are presented below (Figure S1).

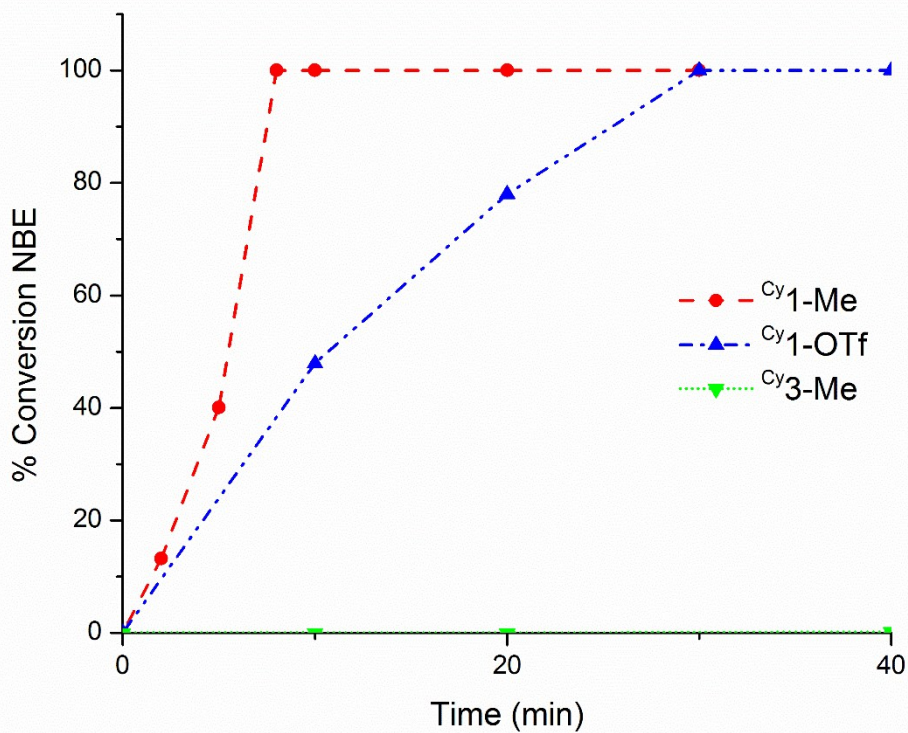


Figure S1. Comparison of Catalyst Activities for Norbornene Hydrogenation (0.5% loading of Rh catalyst, 77 mM norbornene in Et₂O under 1 atm H₂)

Hydrogenation of Norbornene under H₂/D₂. Solutions were prepared as above and, after one freeze–pump–thaw cycle, the frozen solution was placed under H₂ (ca. 0.35 atm) at 77 K, sealed, and then opened briefly to D₂ (ca. 0.70 atm) at 77 K. The vessel was sealed and the reaction allowed to proceed at ambient temperature for 30–45 min, after which an aliquot was analyzed by GC-MS as described above. In Figures S2–S4, partial mass spectra are shown below for samples of norbornene hydrogenated by **Cy1-OTf** under H₂, D₂, and H₂/D₂, showing that norbornene-*d*₁ is the major product formed under H₂/D₂.

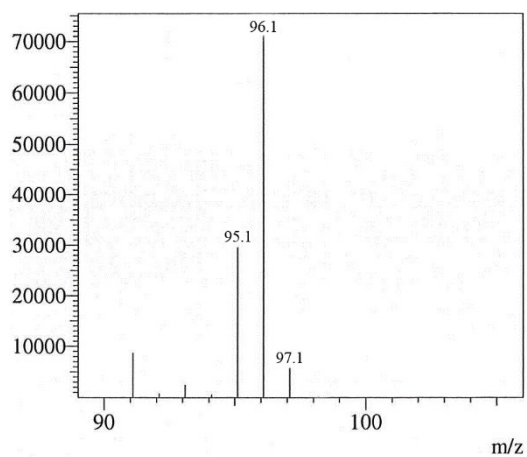


Figure S2. Partial mass spectrum for norbornane- d_0 obtained from hydrogenation of norbornene by **Cy1-OTf** under H₂.

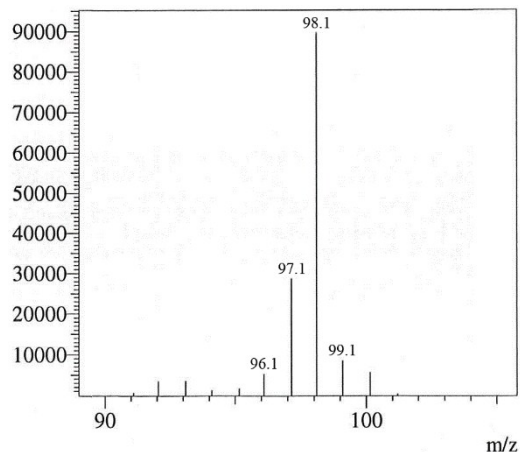


Figure S3. Partial mass spectrum for norbornane- d_2 obtained from hydrogenation of norbornene by **Cy1-OTf** under D₂.

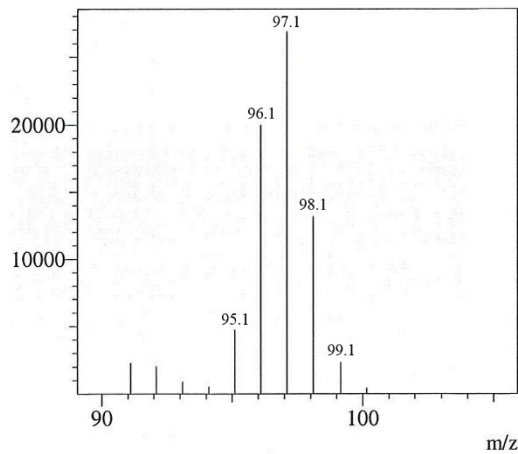


Figure S4. Partial mass spectrum for mixture of norbornane- d_0 , - d_1 , and - d_2 obtained from hydrogenation of norbornene by **Cy1-OTf** under H₂/D₂.

Computational Details. All DFT calculations were performed using Gaussian09⁴ using the M06 functional⁵ and Gaussian's internal LANL2DZ basis set (i.e., LANL2DZ(p,d) double zeta with effective core potentials⁶ for Si, P, S, and Rh and D95V⁷ for H, C, N, O, and F). Geometries were minimized in the gas phase then further optimized with solvent corrections based on the Polarizable Continuum Model (PCM) for benzene using the SCRF module in Gaussian.⁸ Renderings of each complex are presented below along with XYZ coordinates.

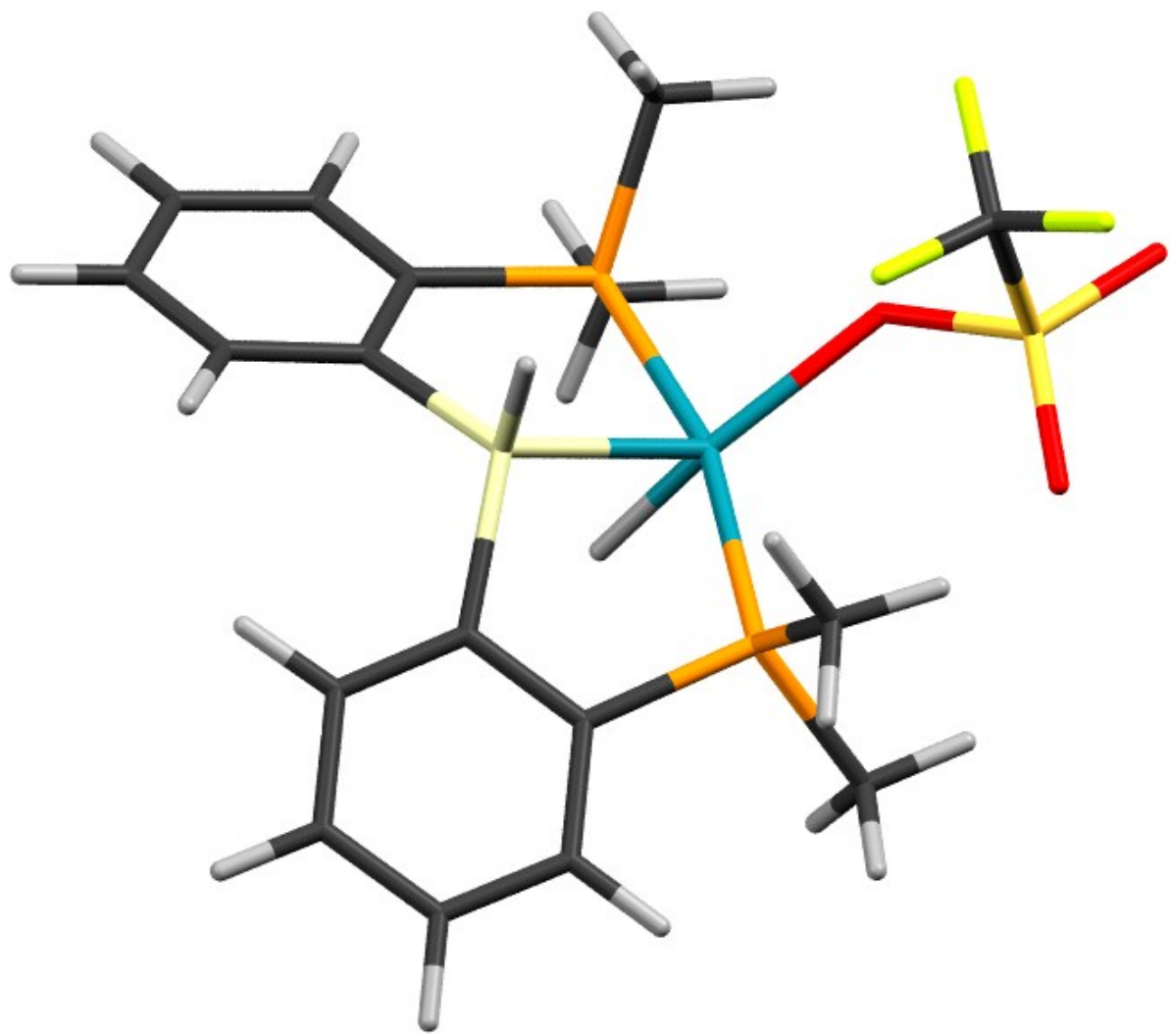


Figure S5. DFT minimized structure of ^{Me}3-H

XYZ Coordinates for Me3-H

Rh	0.00000000	0.00000000	0.00000000
Si	1.69568700	0.38866100	1.56269700
C	2.93615200	-1.05292600	1.45345500
C	4.18099000	-1.06363200	2.11418100
C	5.03113500	-2.17614800	2.03604500
C	4.64163700	-3.30863300	1.30637800
C	3.39715400	-3.32738300	0.66211700
C	2.55317600	-2.20739200	0.73254300
P	0.85976500	-2.21299000	-0.07680700
C	-0.11532900	-3.49424200	0.87361200
H	-0.18467800	-3.17906800	1.91868400
H	0.36701600	-4.47578100	0.81118400
H	-1.12510700	-3.53765200	0.45693100
C	1.11513100	-2.99844900	-1.75432500
H	1.54610500	-4.00005200	-1.65152500
H	1.78071200	-2.36860100	-2.34966300
H	0.14618300	-3.07303900	-2.25516100
H	3.09518200	-4.21529800	0.10923600
H	5.29720300	-4.17203100	1.24717000
H	5.98982200	-2.16211500	2.54577400
H	4.49171500	-0.20561000	2.70705100
C	2.35051800	2.15033800	1.23747700
C	1.43658800	3.04692500	0.63204100
C	1.79349000	4.38120200	0.38951300
C	3.07883100	4.83458000	0.72264800
C	3.99776900	3.95551000	1.31159500
C	3.63071600	2.62636000	1.57502600
H	4.35927600	1.96233700	2.03555500
H	4.99527400	4.30207800	1.56504900
H	3.36075000	5.86346000	0.52038500
H	1.08627400	5.07084200	-0.06775400
P	-0.27745700	2.38255100	0.21551600
C	-0.83900900	3.30547600	-1.30875000
H	-1.83776300	2.93920600	-1.56286600
H	-0.15177300	3.10519200	-2.13461900
H	-0.88890200	4.38252400	-1.11610200
C	-1.31054300	3.14215100	1.58238600
H	-1.02501900	2.69338000	2.53877100
H	-2.36471000	2.93342600	1.37969000
H	-1.12990000	4.22281100	1.61506900
H	1.08910300	0.37511200	2.93597800
O	-1.91962900	-0.93438700	0.18708700
S	-3.39786600	-0.23252800	0.37794400
O	-4.60131500	-1.10917000	-0.19426000
O	-3.40444600	1.34478600	0.09146300
C	-3.54988600	-0.37210200	2.34663100
F	-4.72342900	0.18345800	2.77703600
F	-3.51053700	-1.68744600	2.72455100
F	-2.50278400	0.28898200	2.94317800
H	1.33246400	0.41056900	-0.72096100

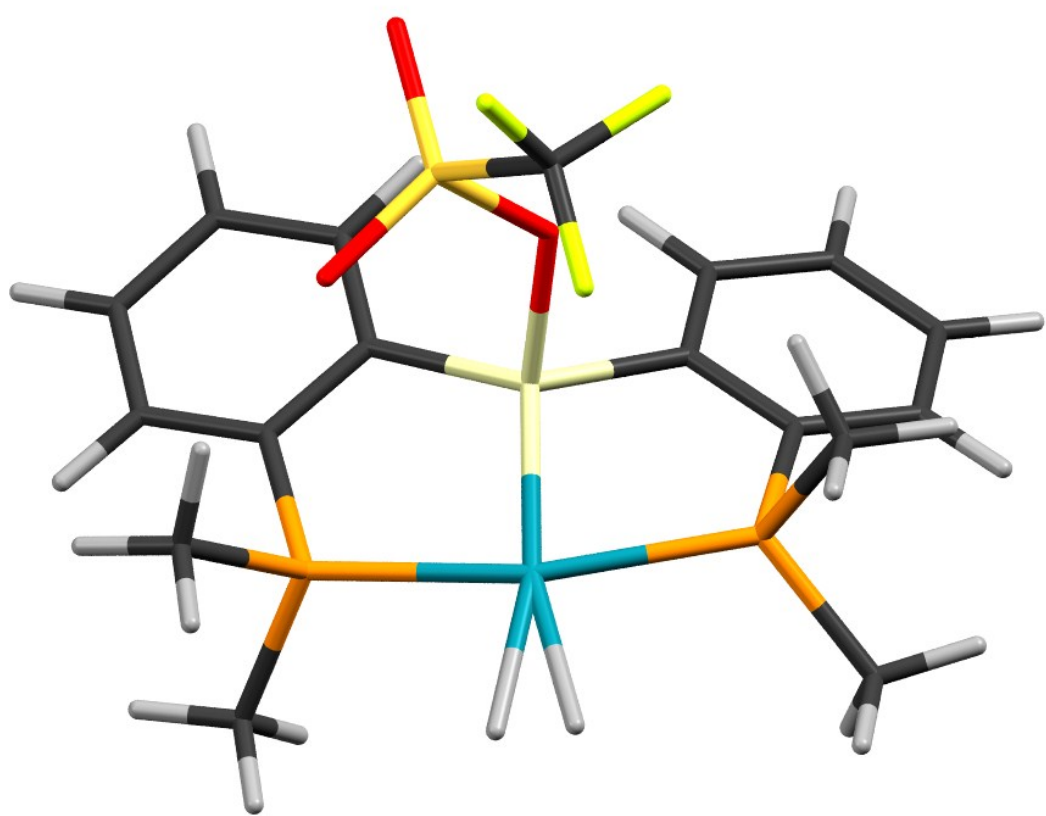


Figure S6. DFT minimized structure of ^{Me}4-OTf

XYZ Coordinates for Me4-OTf

S	0.00000000	0.00000000	0.00000000
O	-1.19154800	-1.07651200	0.49019400
Si	-1.10590000	-2.93669200	0.28489800
Rh	-1.29818300	-3.65160800	-1.88817800
P	-3.60536500	-3.31015100	-1.37928200
C	-3.84369400	-3.40180700	0.49160900
C	-2.68601500	-3.22835800	1.28428400
C	-2.81298300	-3.25455400	2.68498400
H	-1.93778800	-3.12165300	3.31688800
C	-4.06356500	-3.46535700	3.28355600
H	-4.14926100	-3.49568600	4.36561800
C	-5.20562100	-3.63339900	2.48585500
H	-6.17452200	-3.79159900	2.95022600
C	-5.09785000	-3.59460500	1.08755900
H	-5.99149500	-3.71827400	0.47849800
C	-4.38663900	-1.64382400	-1.76278100
H	-4.32451300	-1.44308100	-2.83611300
H	-3.82628600	-0.87370900	-1.22275600
H	-5.43356800	-1.62995500	-1.43852100
C	-4.87187300	-4.51889900	-2.05615400
H	-5.88801400	-4.23506800	-1.76102200
H	-4.80327900	-4.52215400	-3.14799600
H	-4.64593200	-5.52099900	-1.68167800
P	1.03016300	-4.09734600	-1.58828100
C	1.54487500	-3.82042200	0.20672000
C	0.57675300	-3.27016900	1.07405300
C	0.94960500	-2.94285000	2.39229300
H	0.23604100	-2.46060200	3.05774800
C	2.25015400	-3.19899900	2.84862500
H	2.53015300	-2.94044900	3.86534900
C	3.19473700	-3.77595700	1.98613700
H	4.20283800	-3.97254700	2.33874200
C	2.84681500	-4.07620600	0.66077700
H	3.59844700	-4.49417400	-0.00633100
C	2.29998000	-3.10121200	-2.54441000
H	2.12534900	-3.23625000	-3.61612400
H	3.31725900	-3.42313800	-2.29533500
H	2.16447200	-2.04809200	-2.28035000
C	1.56192600	-5.86817200	-1.92272500
H	2.63037500	-6.00622400	-1.72340900
H	1.35662500	-6.10559700	-2.97125300
H	0.97895200	-6.53884500	-1.28584200
O	0.52769000	0.88884100	1.20510800
O	1.02988100	-0.64820200	-1.03284800
C	-1.18802100	1.14698200	-1.08736500
F	-0.48411700	2.23461700	-1.51848300
F	-2.25487600	1.55920900	-0.34561900
F	-1.62832400	0.43317500	-2.16594100
H	-1.87189200	-4.19335400	-3.59148300
H	-1.06543200	-4.30813300	-3.64388100

X-ray Crystallography. X-ray quality crystals of each complex were grown as described in the Experimental Section, with the exception of previously reported **P^h1-OTf**, which was crystallized by slow evaporation of diethyl ether from a concentrated solution at -35°C .

Single-crystal X-ray diffraction data for compounds **C^yP₂SiH₂**, **P^h1-OTf**, and **P^h2** were collected at 173 K on a Rigaku XtaLAB mini diffractometer using Mo K α radiation ($\lambda = 0.71073 \text{ \AA}$). The diffractometer was equipped with an Oxford Cryosystems desktop cooler (Oxford Cryosystems Ltd, Oxford) for low-temperature data collection. The crystals were mounted on a MiTeGen micromount (MiTeGen, LLC, Ithaca, NY) using STP oil. The frames were integrated using CrystalClear-SM Expert 3.1 b27⁹ to give the *hkl* files corrected for *Lp* and decay. Data were corrected for absorption effects using a multiscan method (REQAB).⁹

Single-crystal X-ray diffraction data for compound **C^y1-OTf** were collected at 100 K at the Bruker AXS, Inc. X-ray crystallographic laboratory on a Bruker D8 QUEST ECO diffractometer using Mo K α radiation ($\lambda = 0.71073 \text{ \AA}$). The data intensities were corrected for absorption and decay (SADABS). Final cell constants were obtained from least-squares fits of all measured reflections.

All structures were solved using SIR2004 and refined using SHELXL-2014 with the Olex2 software package.¹⁰ All non-hydrogen atoms were refined with anisotropic thermal parameters. Special refinement details for complex **P^h1-OTf** are provided below, and crystallographic parameters of all complexes are summarized in Table S1. ORTEP drawings were prepared using ORTEP-3 for Windows V2013.1¹¹ and POV-Ray for Windows v3.6.¹² Crystallographic data for the complexes have been deposited at the Cambridge Crystallographic Data Centre (Nos. 1444624–1444627) and can be obtained free of charge via www.ccdc.cam.ac.uk.

Special Crystallographic Refinement Details. The triflate units in triflatosilyl complex **Pb1-OTf** were disordered over two positions. In order to allow suitable refinement, the triflate units were restrained using a SAME command.

The hydrogen atoms attached to silicon in the crystal structure of $^{Cy}P_2SiH_2$ ligand were located in the difference map and allowed to refine freely.

The crystal structure of **Pb2** contains voids (580.3 \AA^3) filled with disordered solvent molecules, most likely dichloromethane. Their contribution to structure factors ($134 \text{ e}^-/\text{cell}$) was modeled using PLATON SQUEEZE.¹³ Since the identity of molecules occupying the void is not definitive, we have conservatively omitted them from the reported formulae in refinement and the CIF.

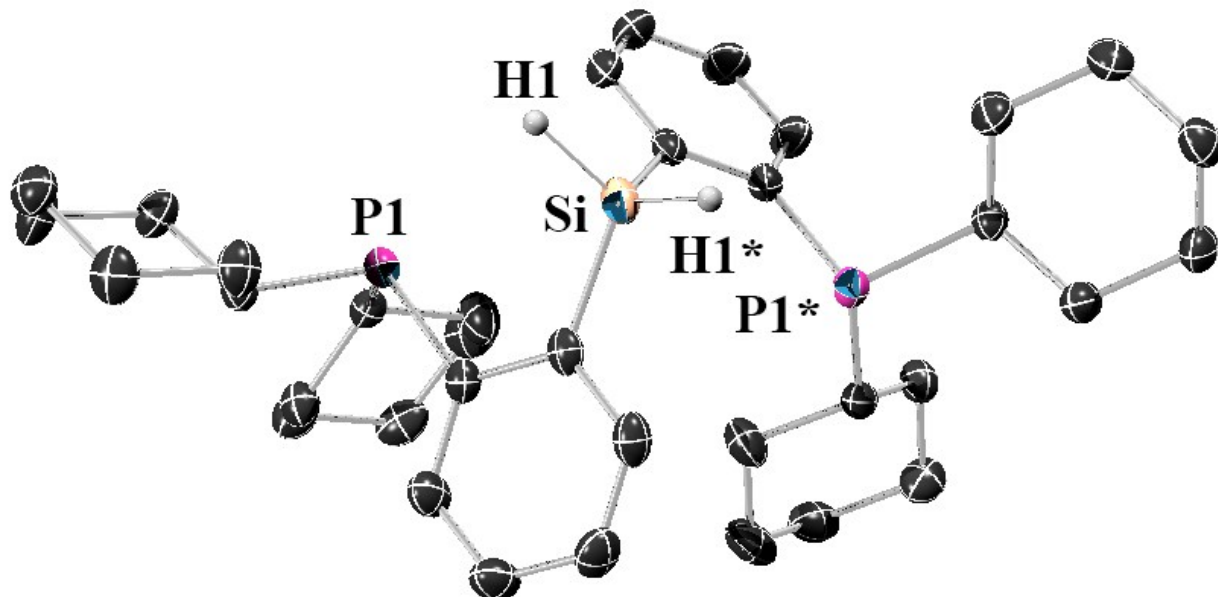


Figure S7. Crystal structure of $^{Cy}P_2SiH_2$ with thermal ellipsoids at the 50% probability level and hydrogen atoms omitted for clarity.

Table S1. X-ray crystallographic data

complex	c_yP₂SiH₂	P^h1-OTf	c_y1-OTf	P^h2
Empirical Formula	C ₃₆ H ₅₄ P ₂ Si	C ₄₄ H ₃₆ F ₃ O ₃ P ₂ RhSSi	C ₄₄ H ₆₀ F ₃ O ₃ P ₂ RhSSi	C ₇₄ H ₅₆ F ₆ O ₆ P ₄ Rh ₂ S ₂ Si ₂
Formula Weight	576.82	894.73	918.92	1605.18
T (K)	173(2)	173(2)	100(2)	173(2)
Crystal System	Monoclinic	Monoclinic	Orthorhombic	Monoclinic
Space Group	C2/c	P2 ₁ /n	P2 ₁ 2 ₁ 2 ₁	P2 ₁ /n
a (Å)	15.139(2)	10.9558(12)	11.5434(5)	13.2957(14)
b (Å)	9.8506(13)	16.9365(18)	17.6337(7)	13.9009(15)
c (Å)	22.244(3)	20.550(2)	20.4488(8)	20.145(2)
α (deg)	90	90	90	90
β (deg)	92.736(7)	96.203(7)	90	97.111(7)
γ (deg)	90	90	90	90
V (Å ³)	3313.4(8)	3790.8(7)	4162.4(3)	3353.5(11)
Z	4	4	4	2
d _{calc} (g/cm ³)	1.156	1.568	1.466	1.443
μ (mm ⁻¹)	0.190	0.679	0.620	0.687
Reflections Collected	3811	35554	74846	36379
Independent Reflections	3811 [R(int) = 0.0398]	7747 [R(int) = 0.0919]	8519 [R(int) = 0.0905]	8451 [R(int) = 0.0548]
Data / Restraints / Parameters	3811 / 0 / 181	7747 / 15 / 560	8519 / 382 / 496	8451 / 0 / 433
GOF on F ²	1.073	1.052	1.066	1.048
R1 (wR2)	0.0546 (0.1169)	0.0516 (0.1067)	0.0384 (0.0724)	0.0392 (0.0954)

CyP₂SiH₂ ligand - ¹H NMR

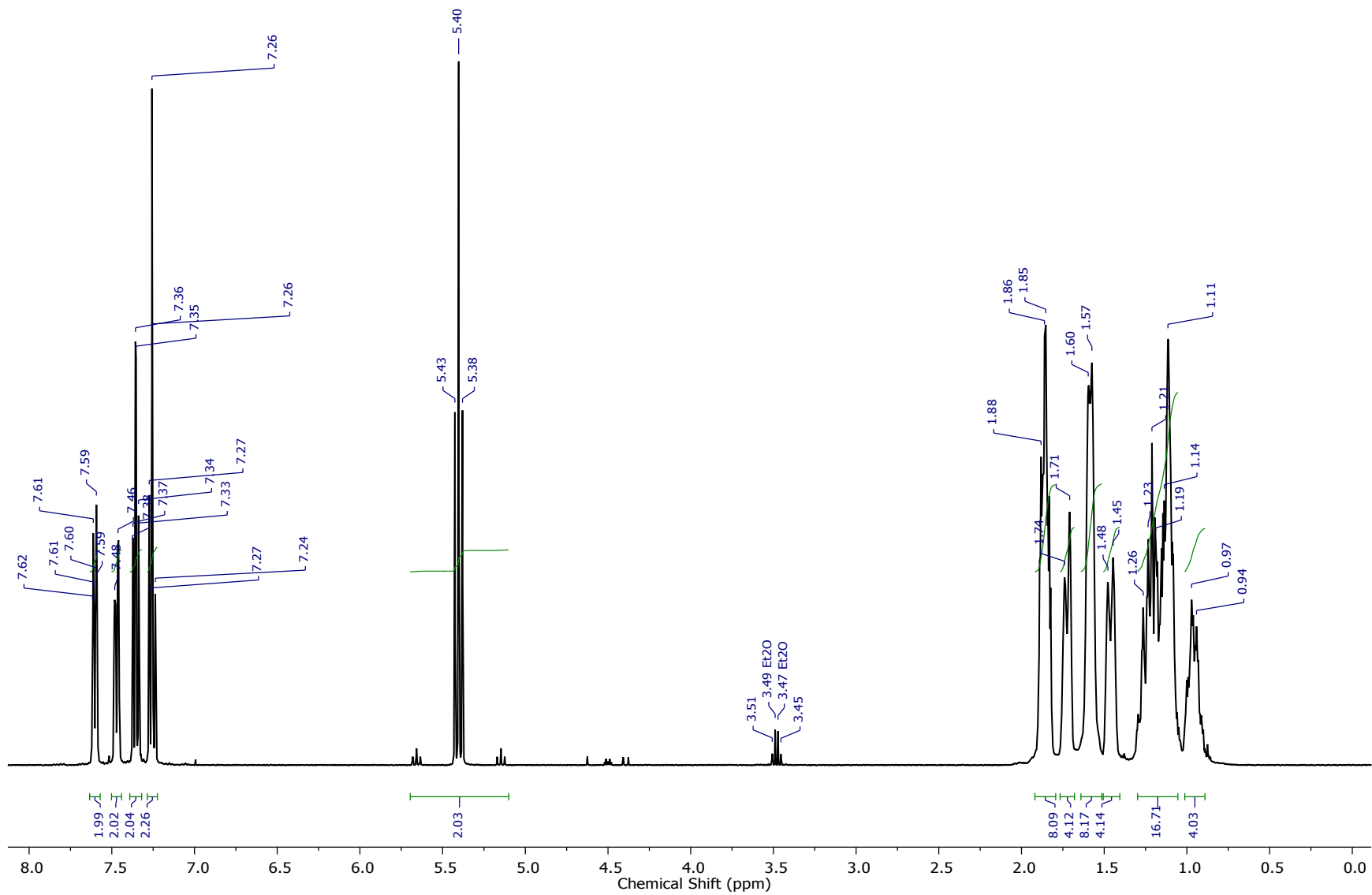


Figure S8. ¹H NMR spectrum of CyP₂SiH₂ in CDCl₃

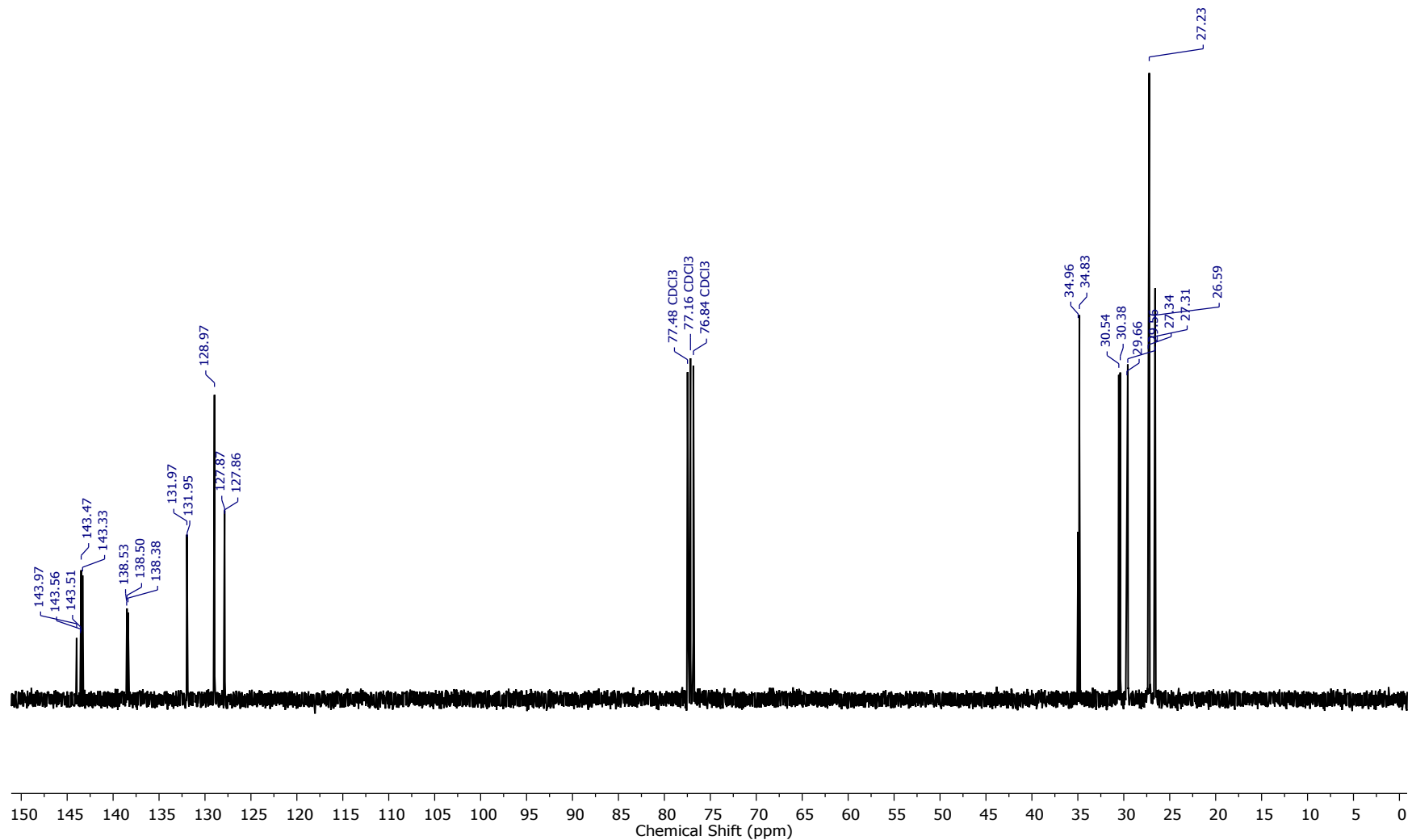


Figure S9. ¹³C NMR spectrum of CyP₂SiH₂ in CDCl₃

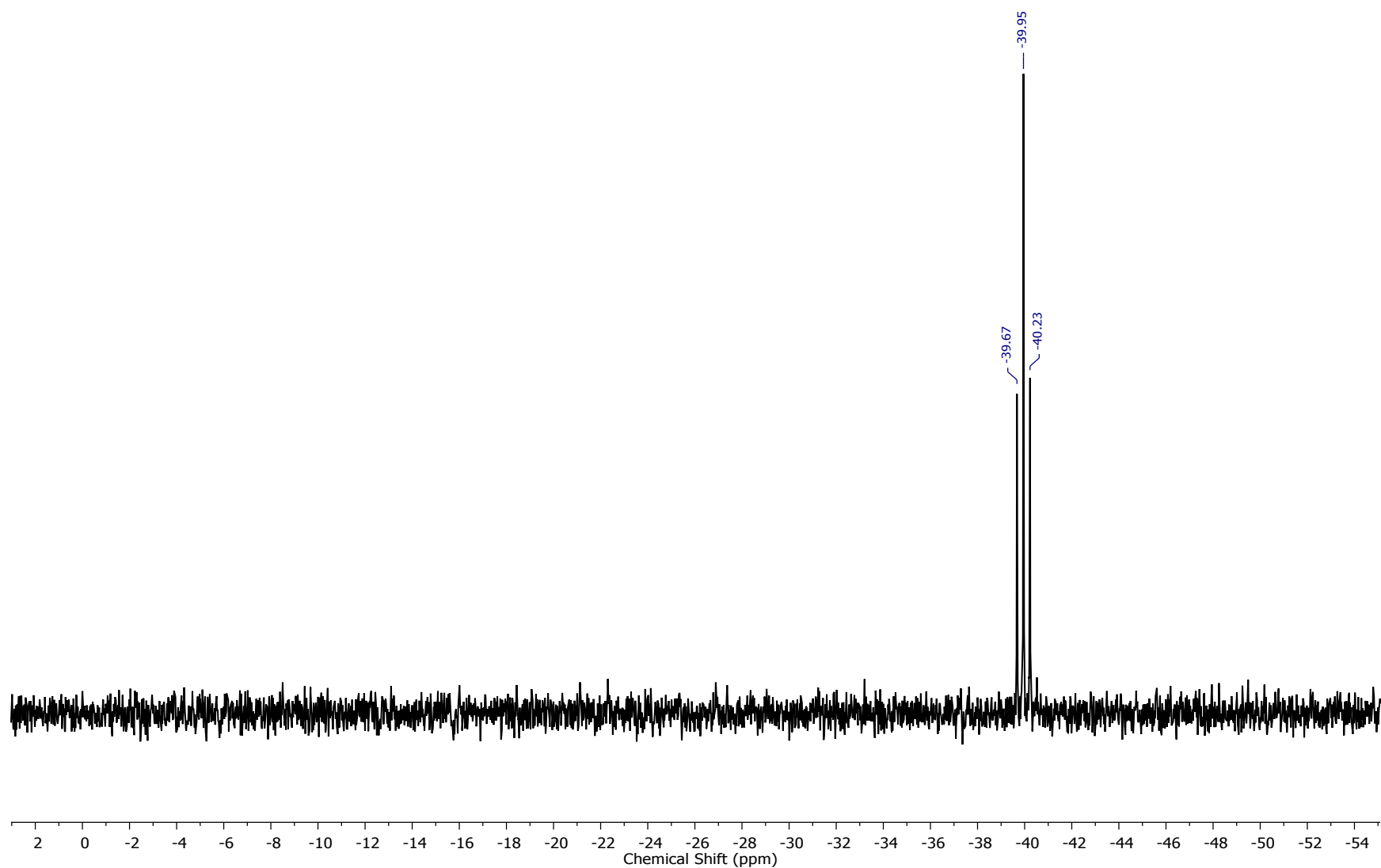


Figure S10. ²⁹Si NMR spectrum of CyP₂SiH₂ in CDCl₃

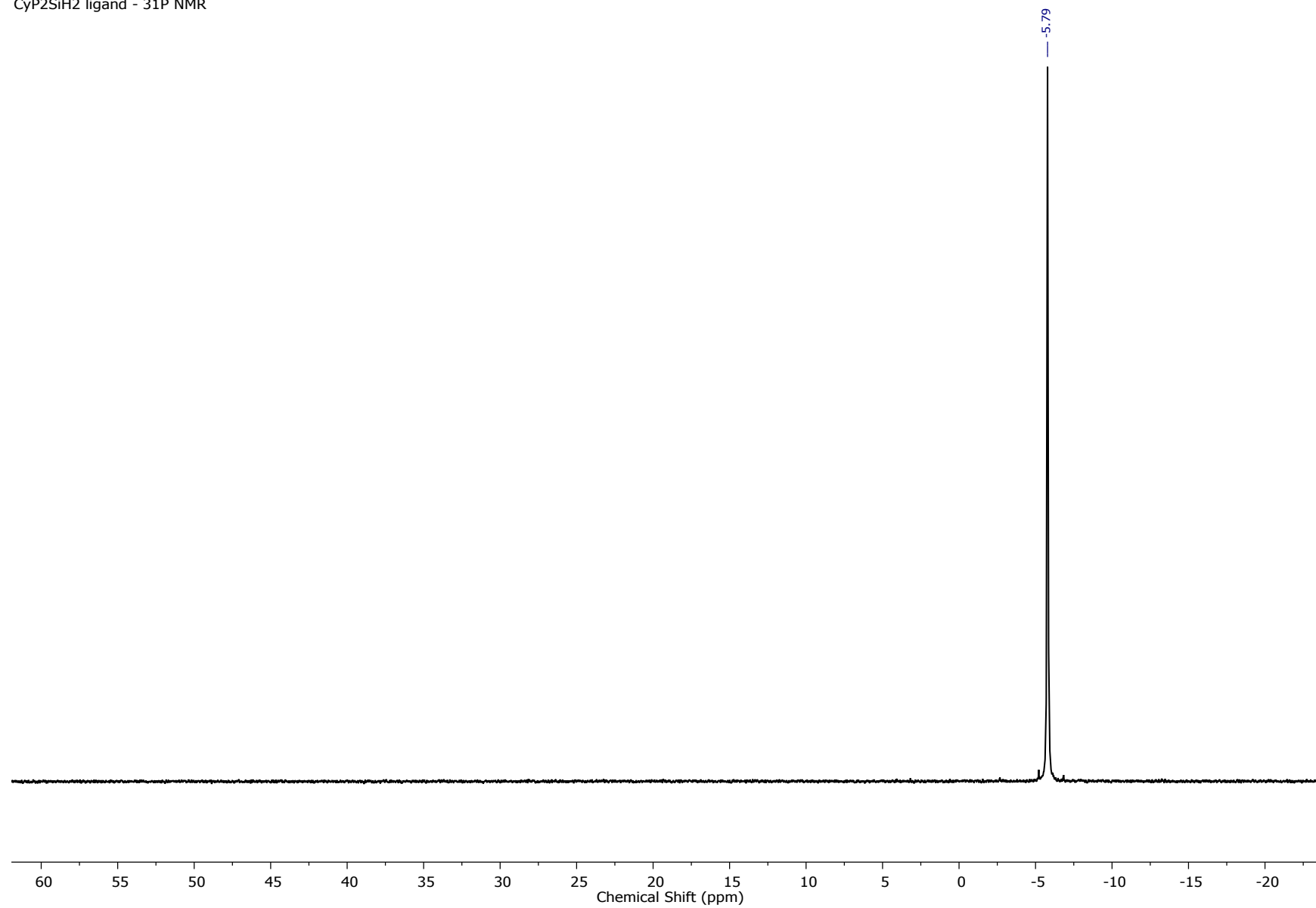


Figure S11. ³¹P NMR spectrum of CyP₂SiH₂ in CDCl₃

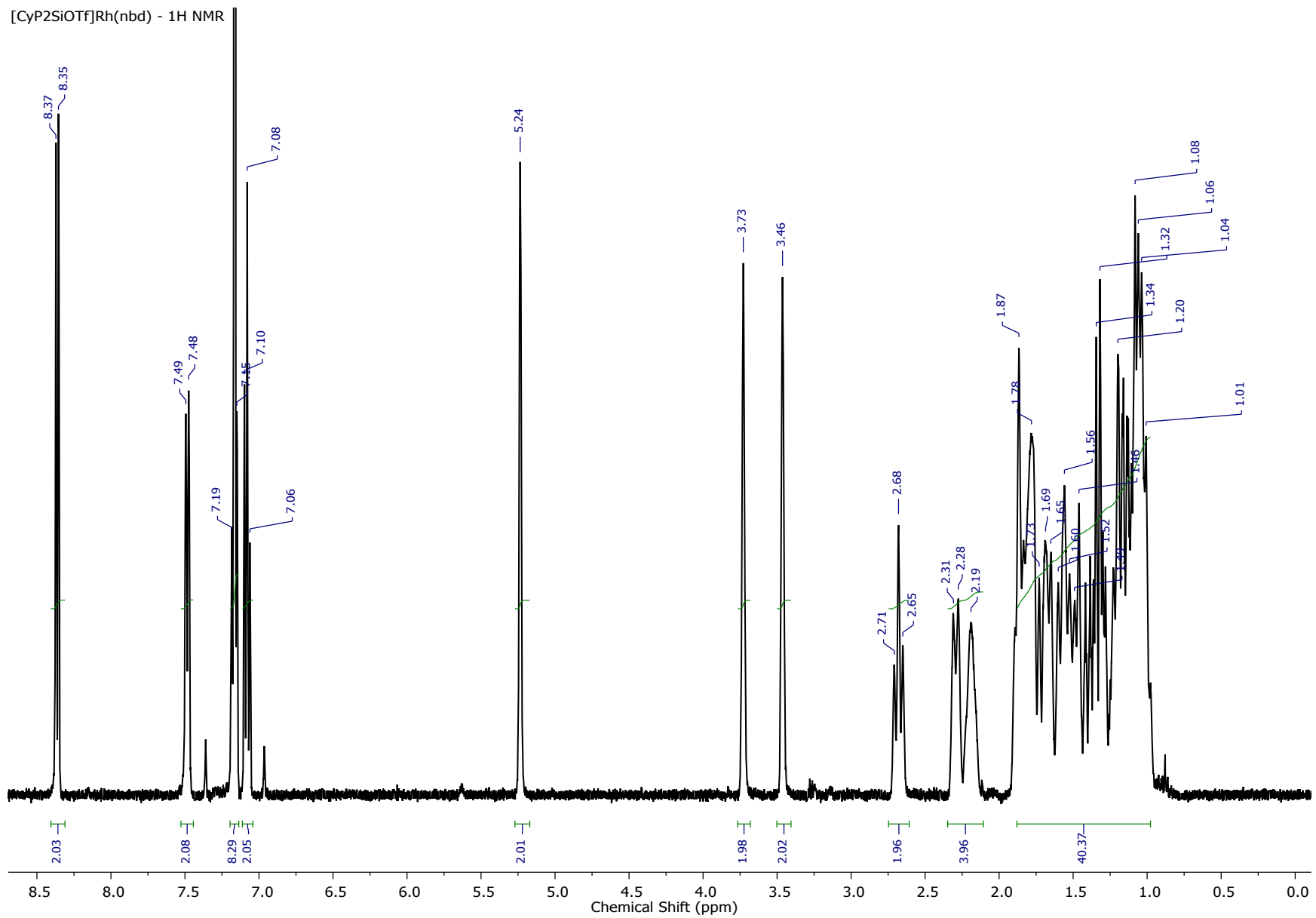


Figure S12. ¹H NMR spectrum of [CyP₂SiOTf]Rh(nbd) (**Cy1-OTf**) in C₆D₆

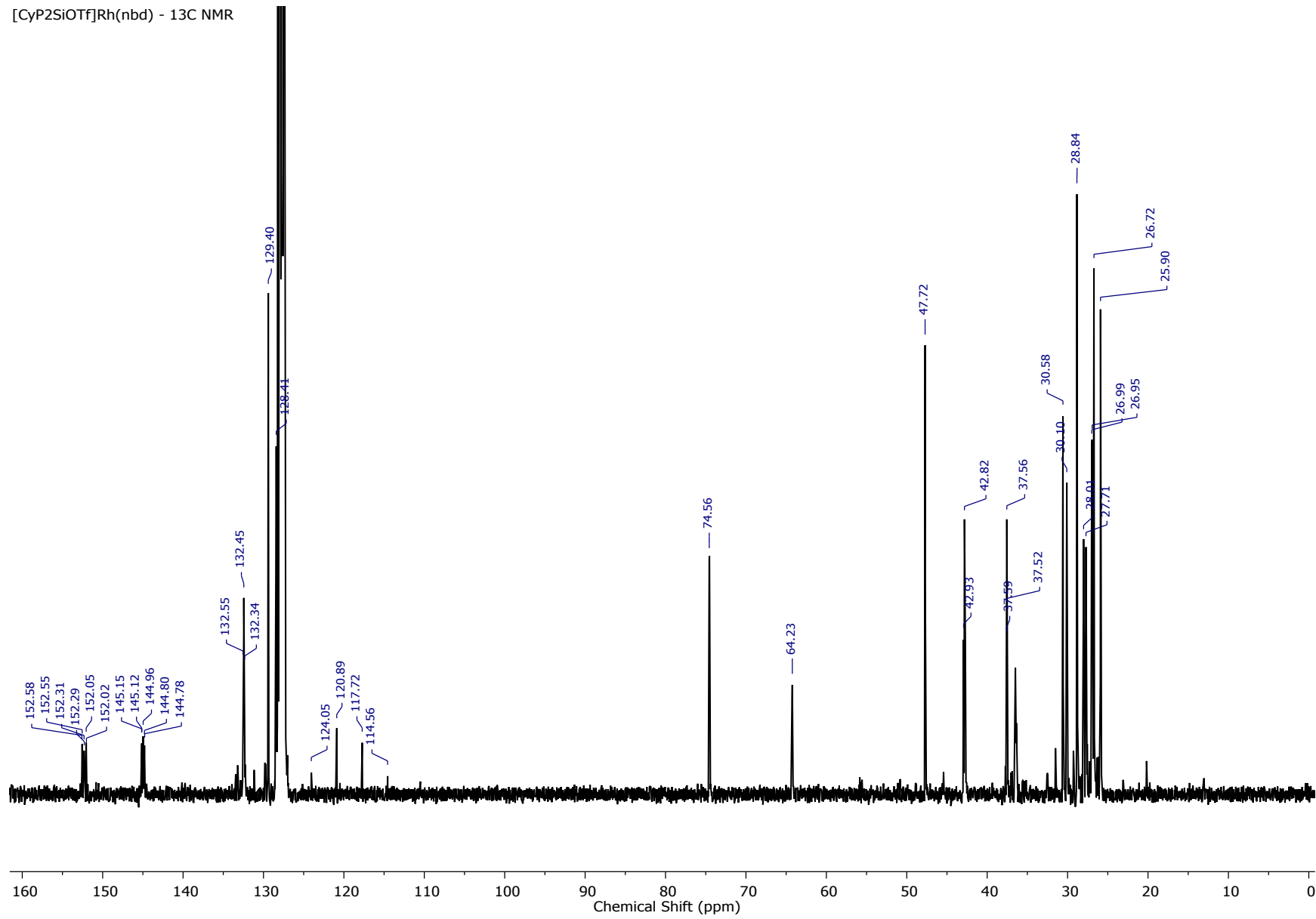


Figure S13. ¹³C NMR spectrum of [CyP₂SiOTf]Rh(nbd) (**Cy1-OTf**) in C₆D₆

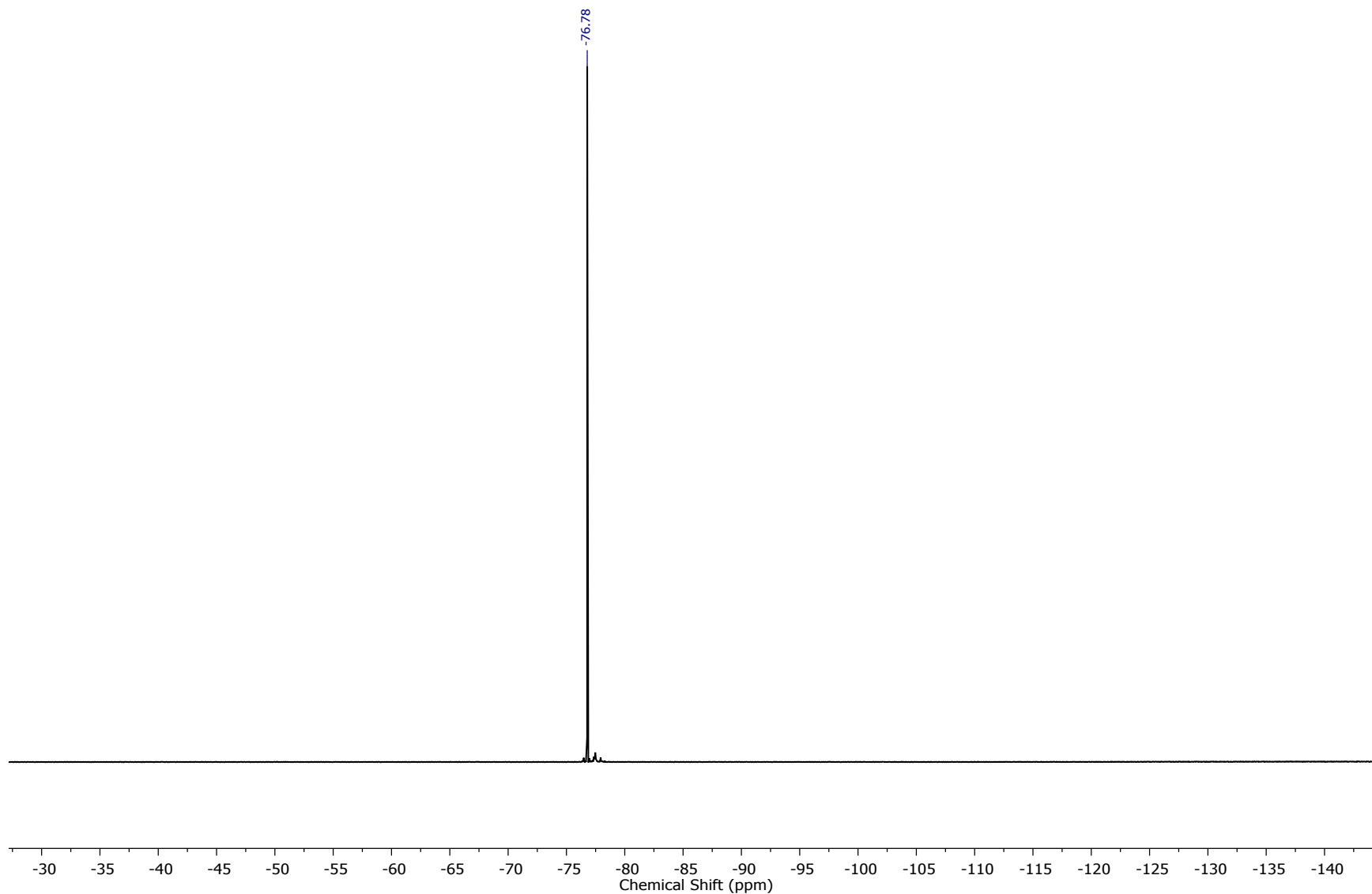


Figure S14. ¹⁹F NMR spectrum of [CyP₂SiOTf]Rh(nbd) (**Cy1-OTf**) in C₆D₆

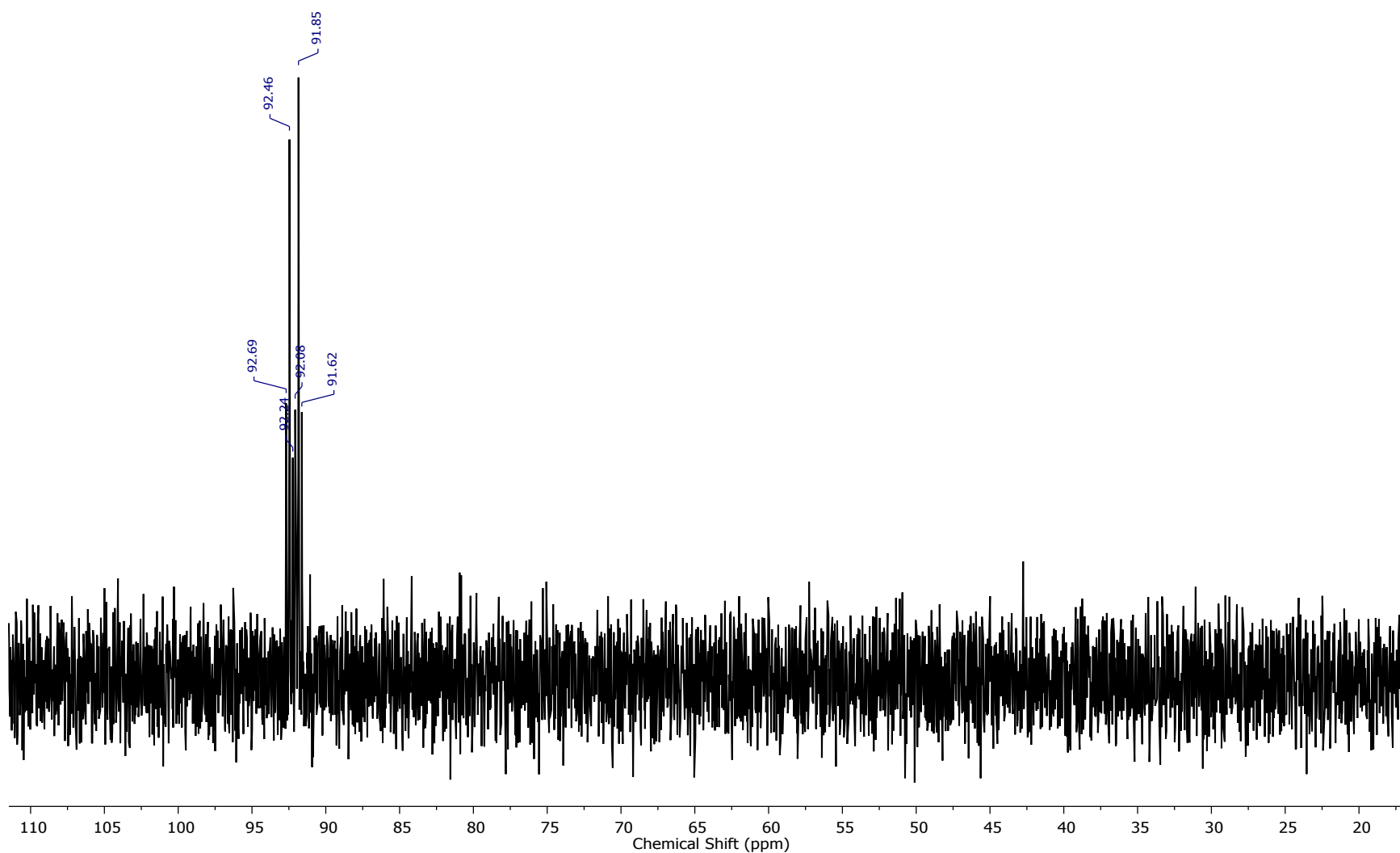


Figure S15. ²⁹Si NMR spectrum of [CyP₂SiOTf]Rh(nbd) (**Cy1-OTf**) in C₆D₆

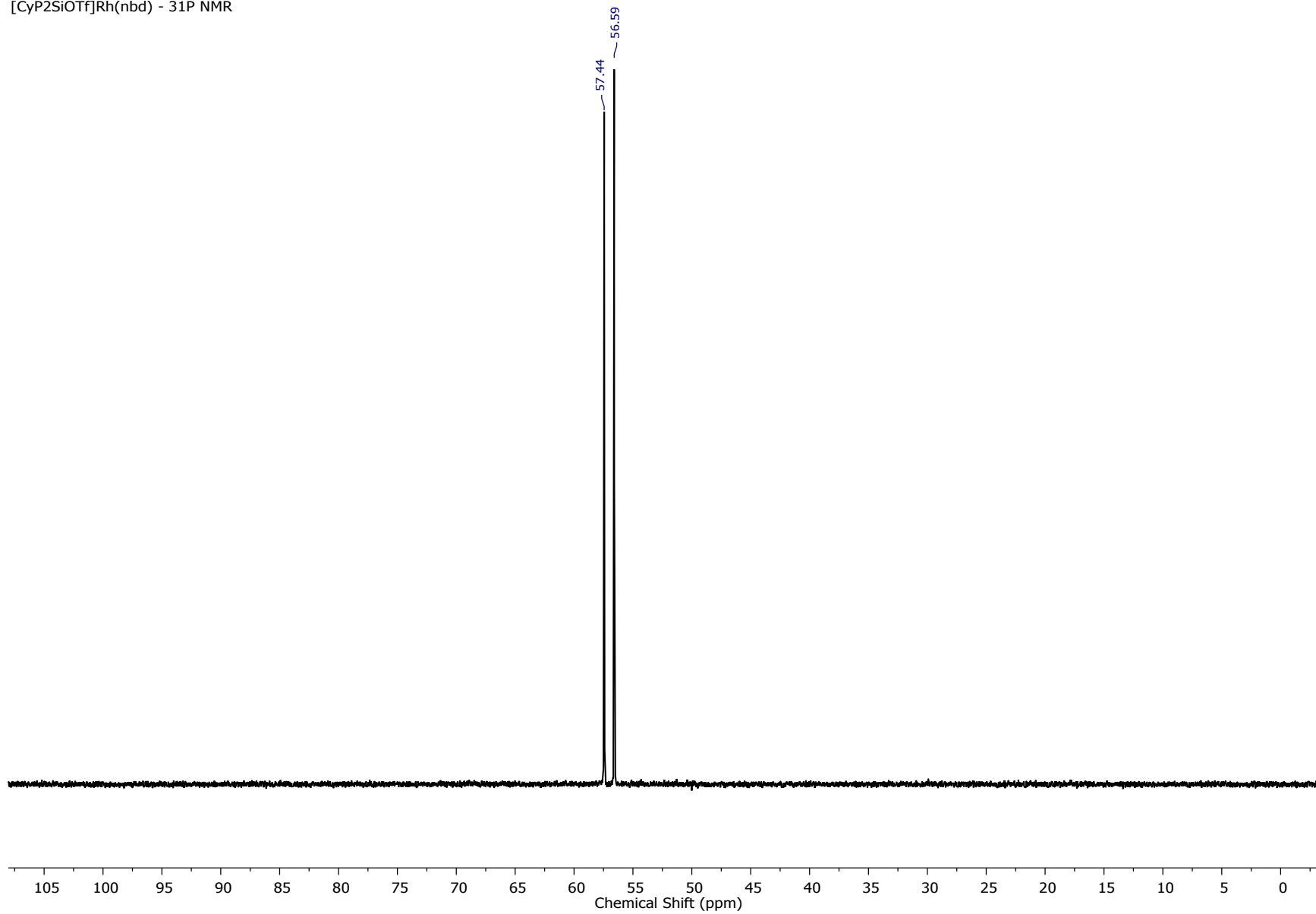


Figure S16. ³¹P NMR spectrum of [CyP₂SiOTf]Rh(nbd) (**Cy1-OTf**) in C₆D₆

[CyP₂SiOTf]Rh(nbd) - ²⁹Si NMR after 24h in solution (~30% decomp)

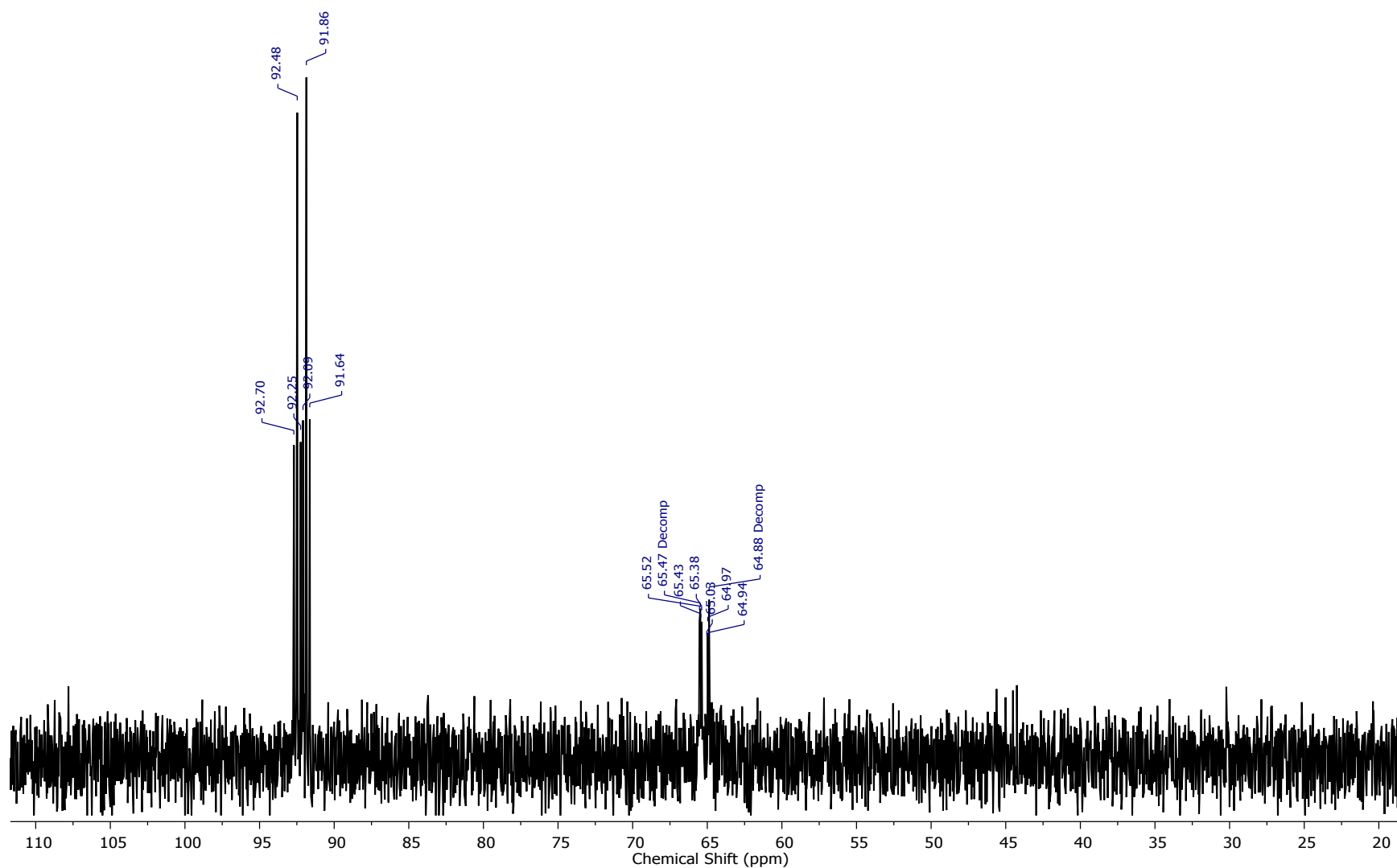


Figure S17. ²⁹Si NMR spectrum of [CyP₂SiOTf]Rh(nbd) (**Cy1-OTf**) in ⁶D₆ after partial decomposition

[CyP₂SiOTf]Rh(nbd) - ³¹P NMR after 48h in solution (~40% decomp)

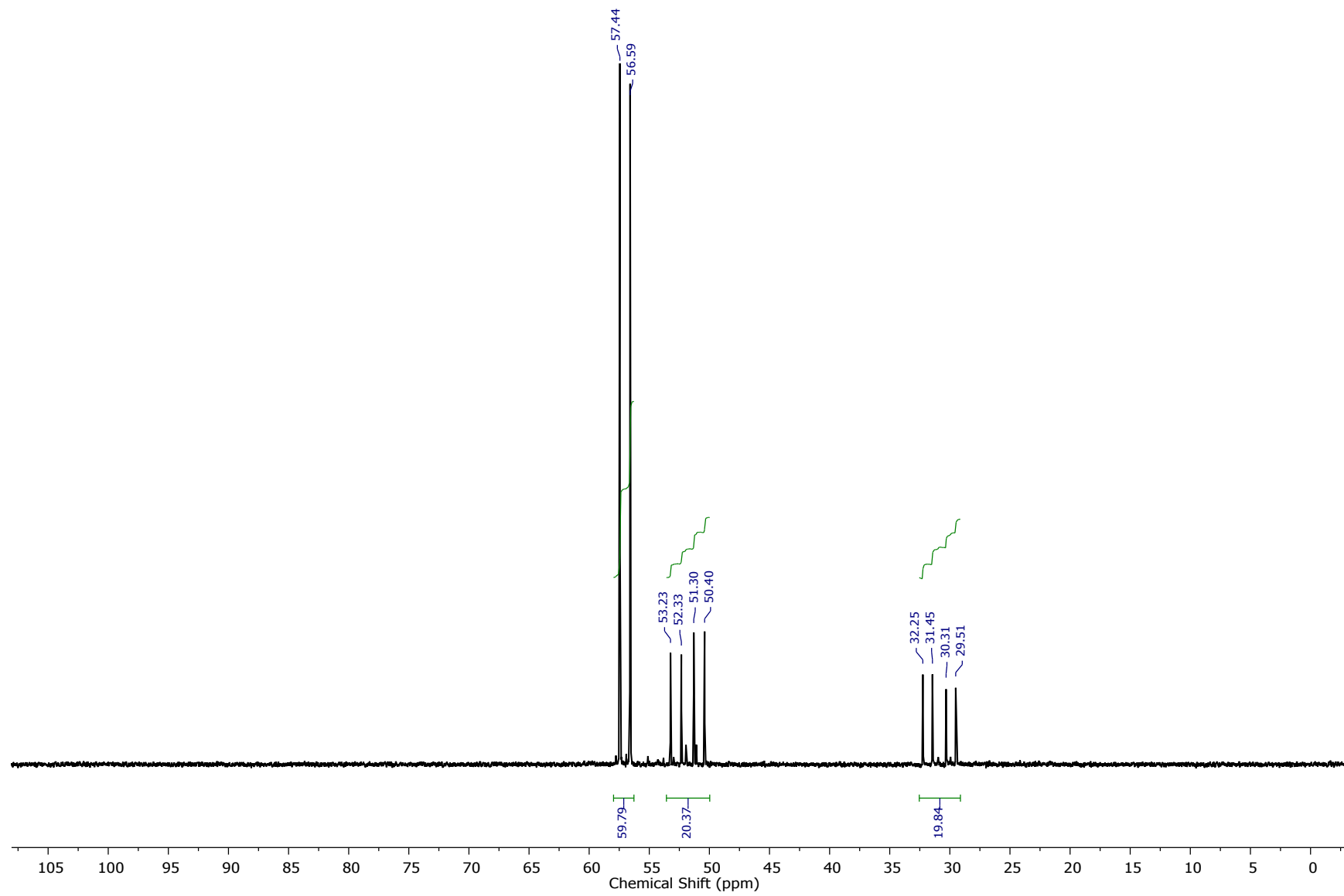


Figure S18. ³¹P NMR spectrum of [CyP₂SiOTf]Rh(nbd) (**Cy1-OTf**) in C₆D₆ after partial decomposition

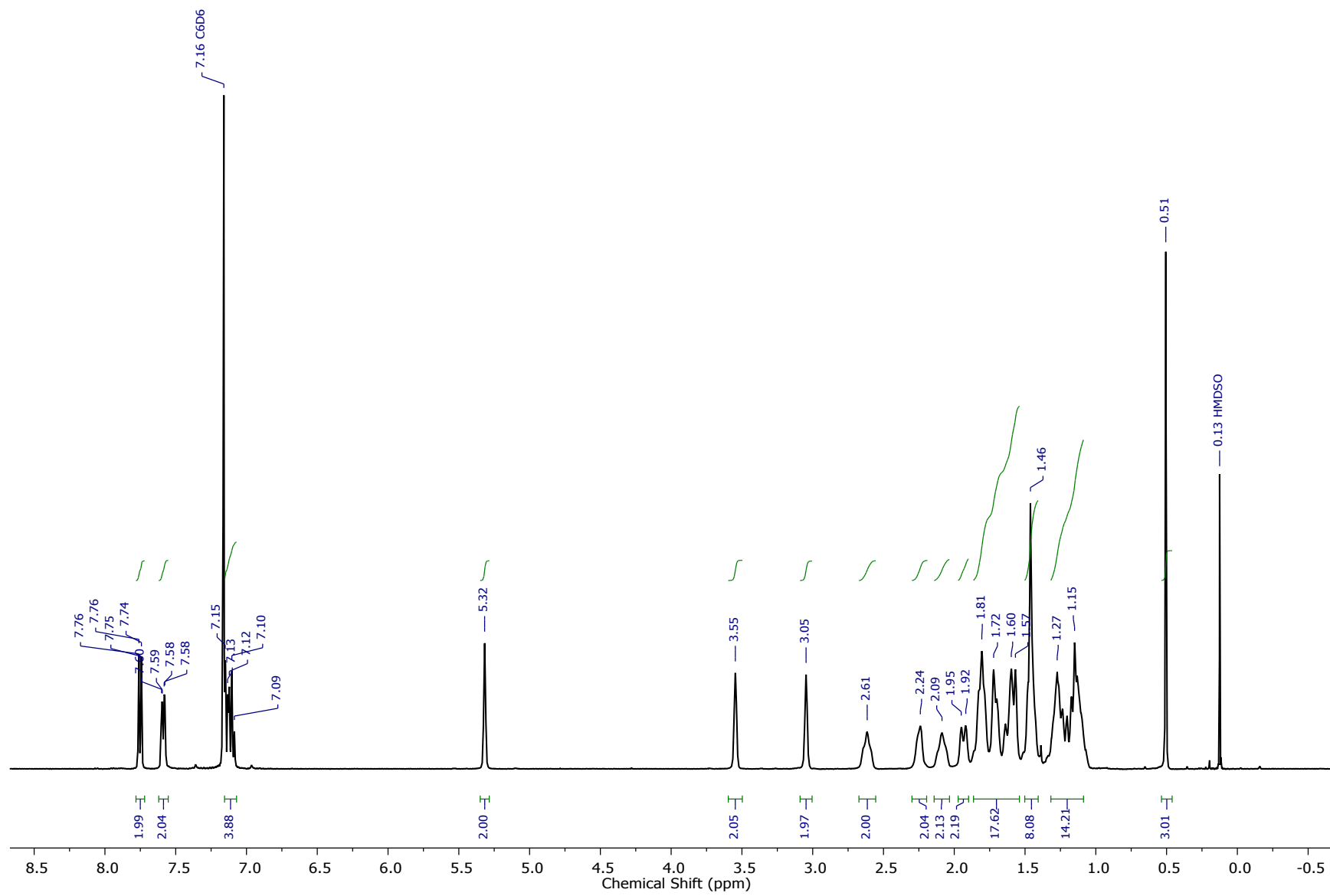


Figure S19. ^1H NMR spectrum of $[\text{CyP}_2\text{SiMe}]\text{Rh}(\text{nbd})$ (**Cy1-Me**) in C_6D_6

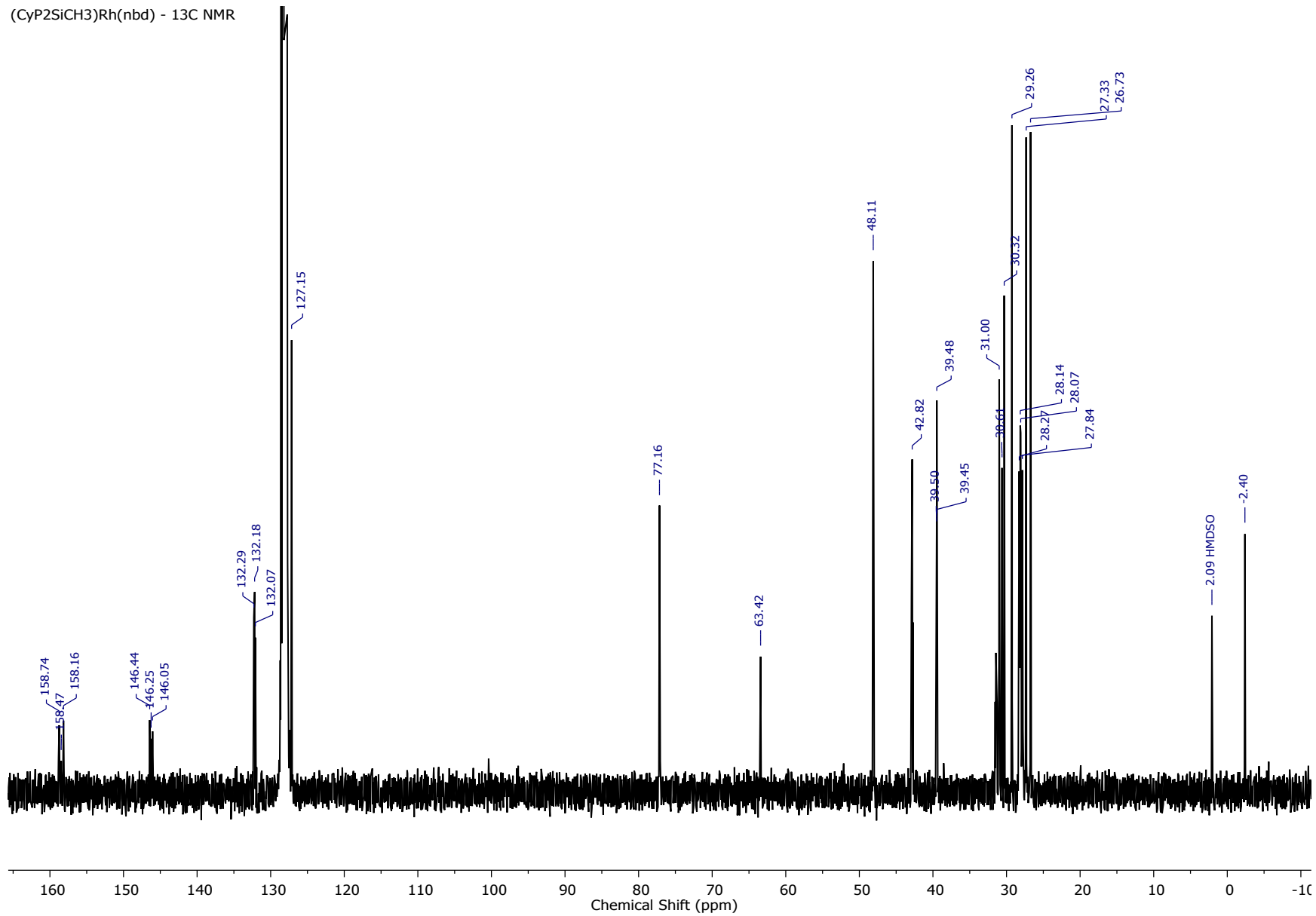


Figure S20. ¹³C NMR spectrum of [CyP₂SiMe]Rh(nbd) (**Cy1-Me**) in C₆D₆

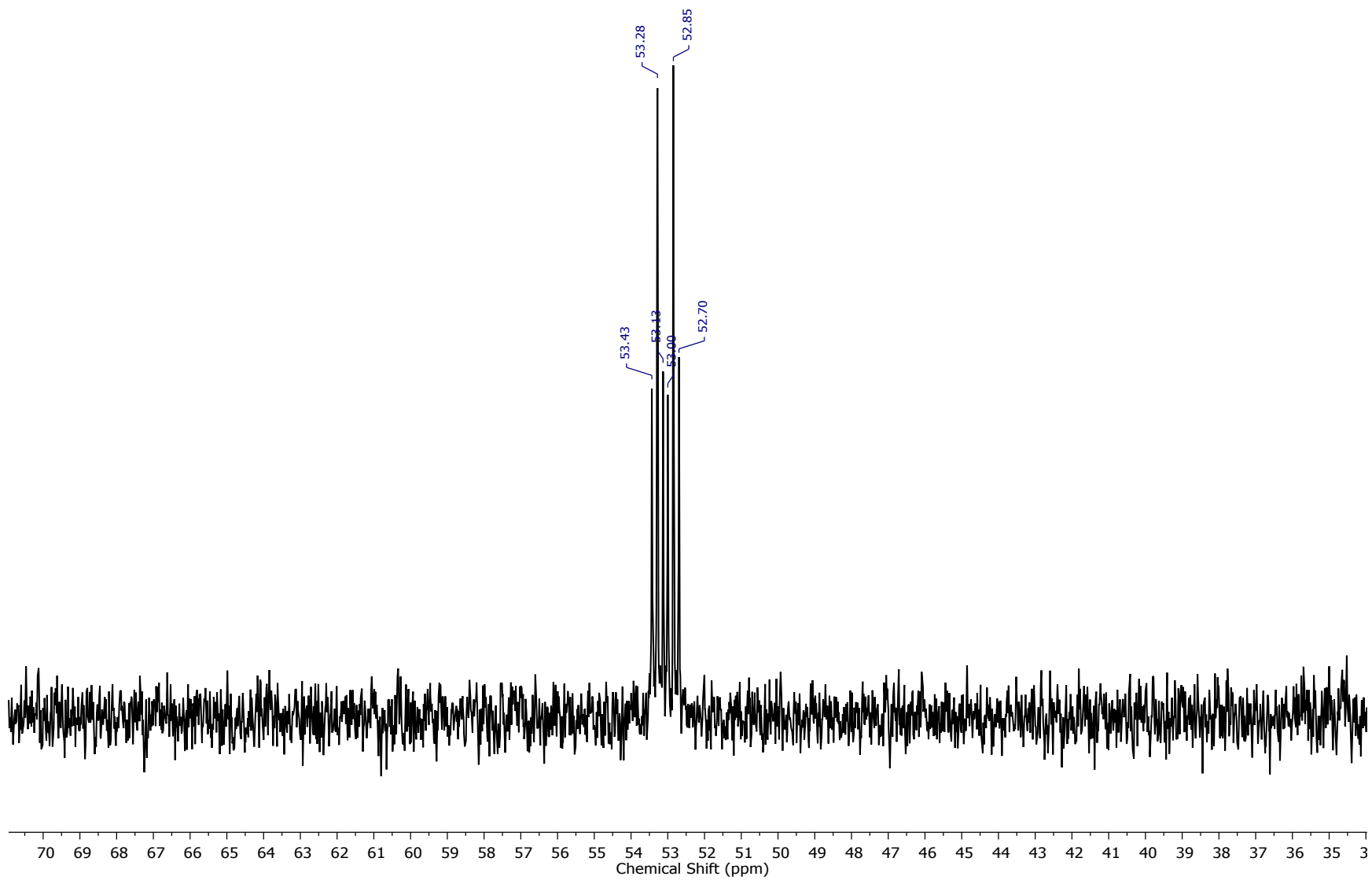


Figure S21. ²⁹Si NMR spectrum of [Cy₂P₂Si^{Me}]Rh(nbd) (**Cy1-Me**) in C₆D₆

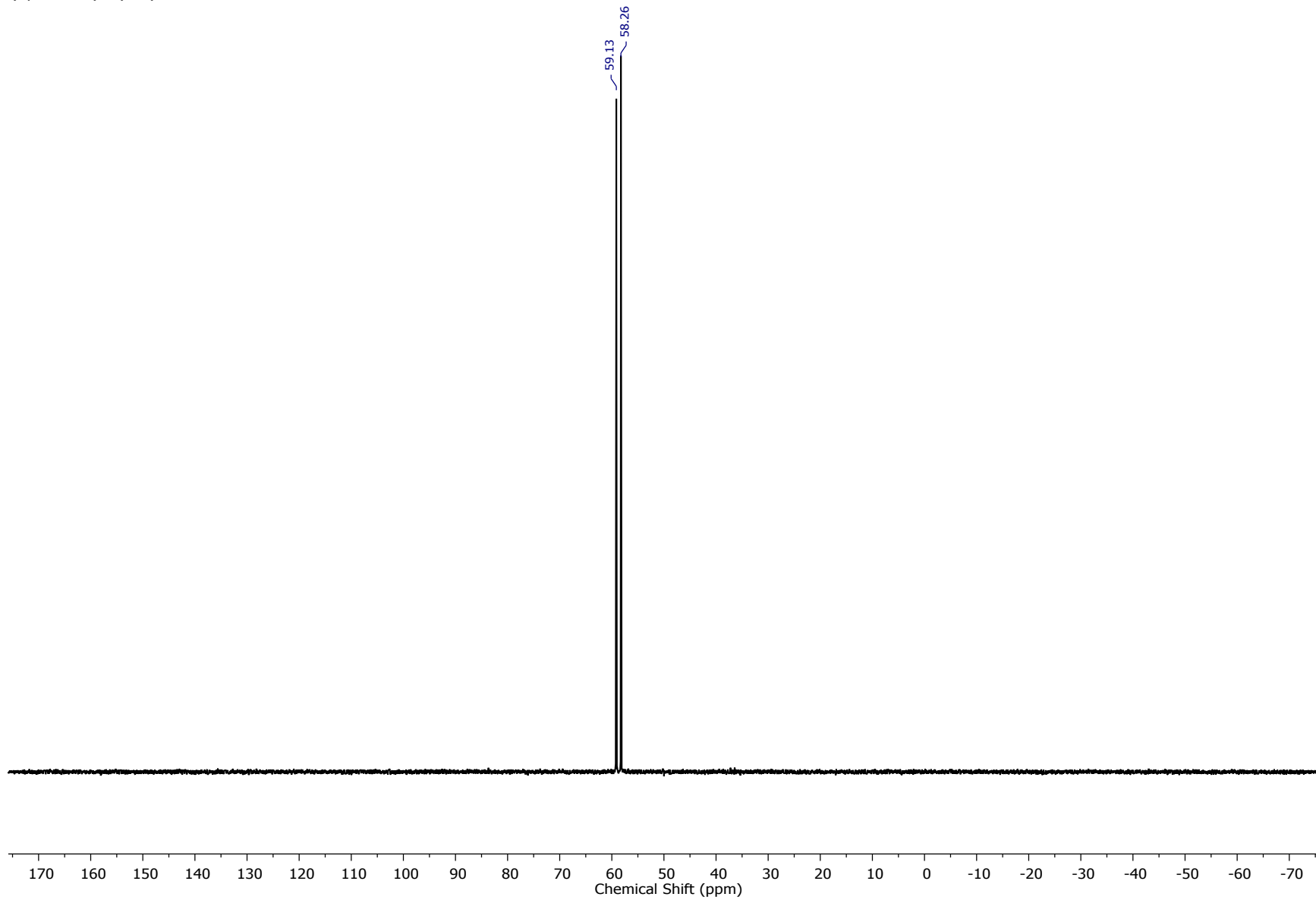


Figure S22. ³¹P NMR spectrum of [CyP₂SiMe]⁺Rh(nbd) (**Cy1-Me**) in C₆D₆

[^{Cy}P₂SiH]Rh(H)(OTf) - ¹H NMR

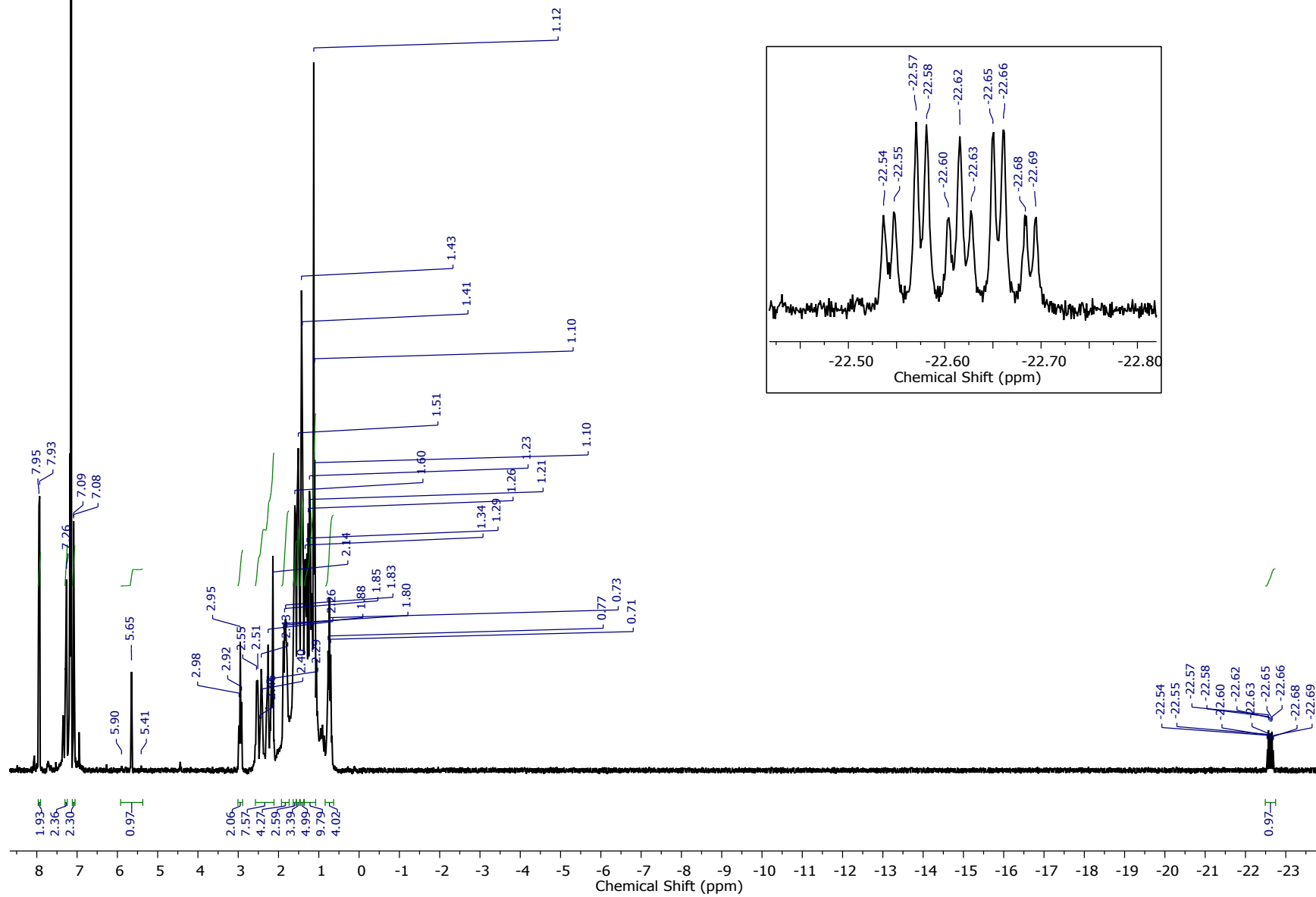


Figure S23. ¹H NMR spectrum of [^{Cy}P₂SiH]Rh(nbd) (^{Cy}3-H) in C₆D₆

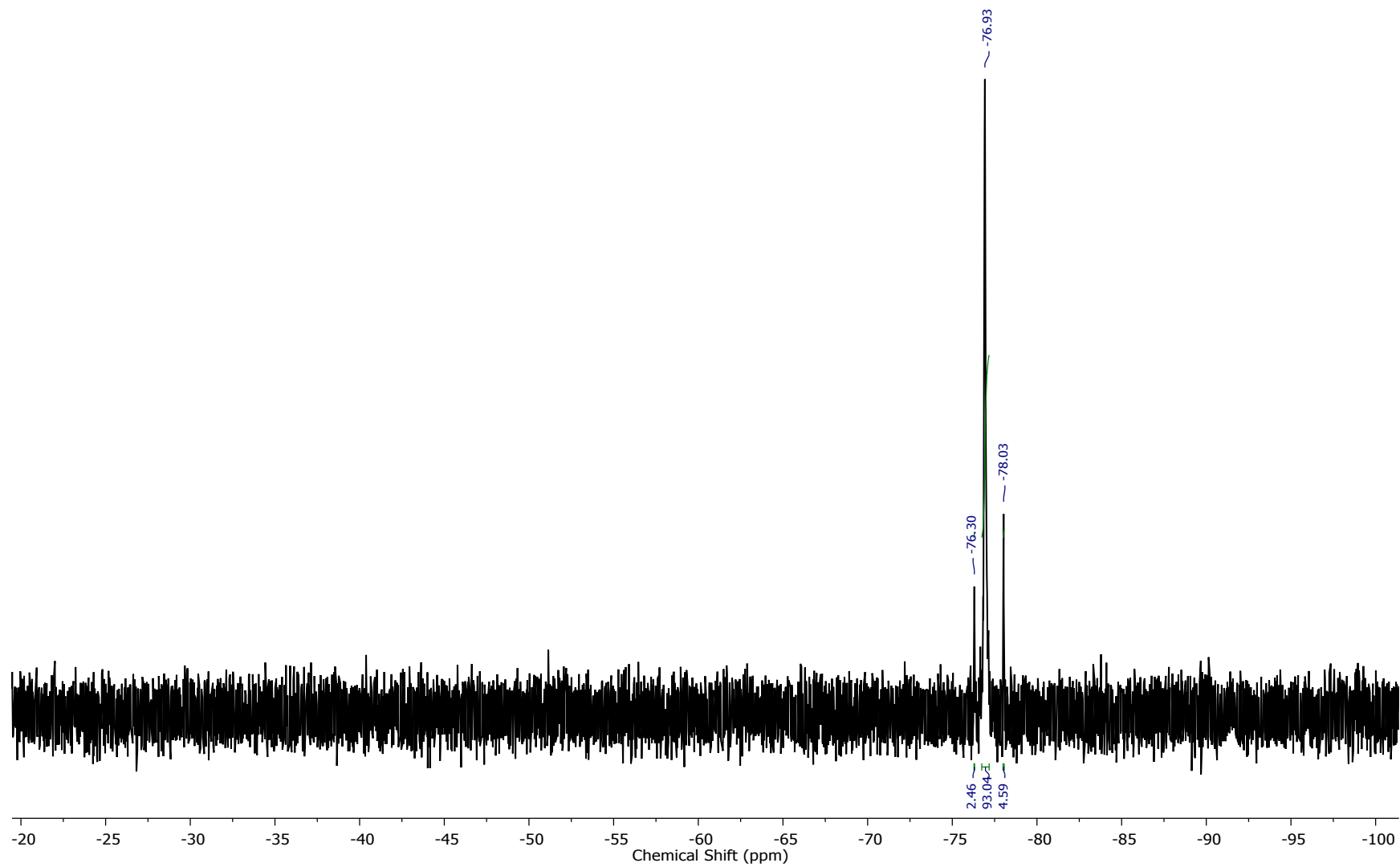


Figure S24. ¹⁹F NMR spectrum of $^{[{\text{Cy}}_2{\text{P}}_2{\text{SiH}}]}{\text{Rh(nbd)}}$ ($^{\text{Cy}3\text{-H}}$) in C_6D_6

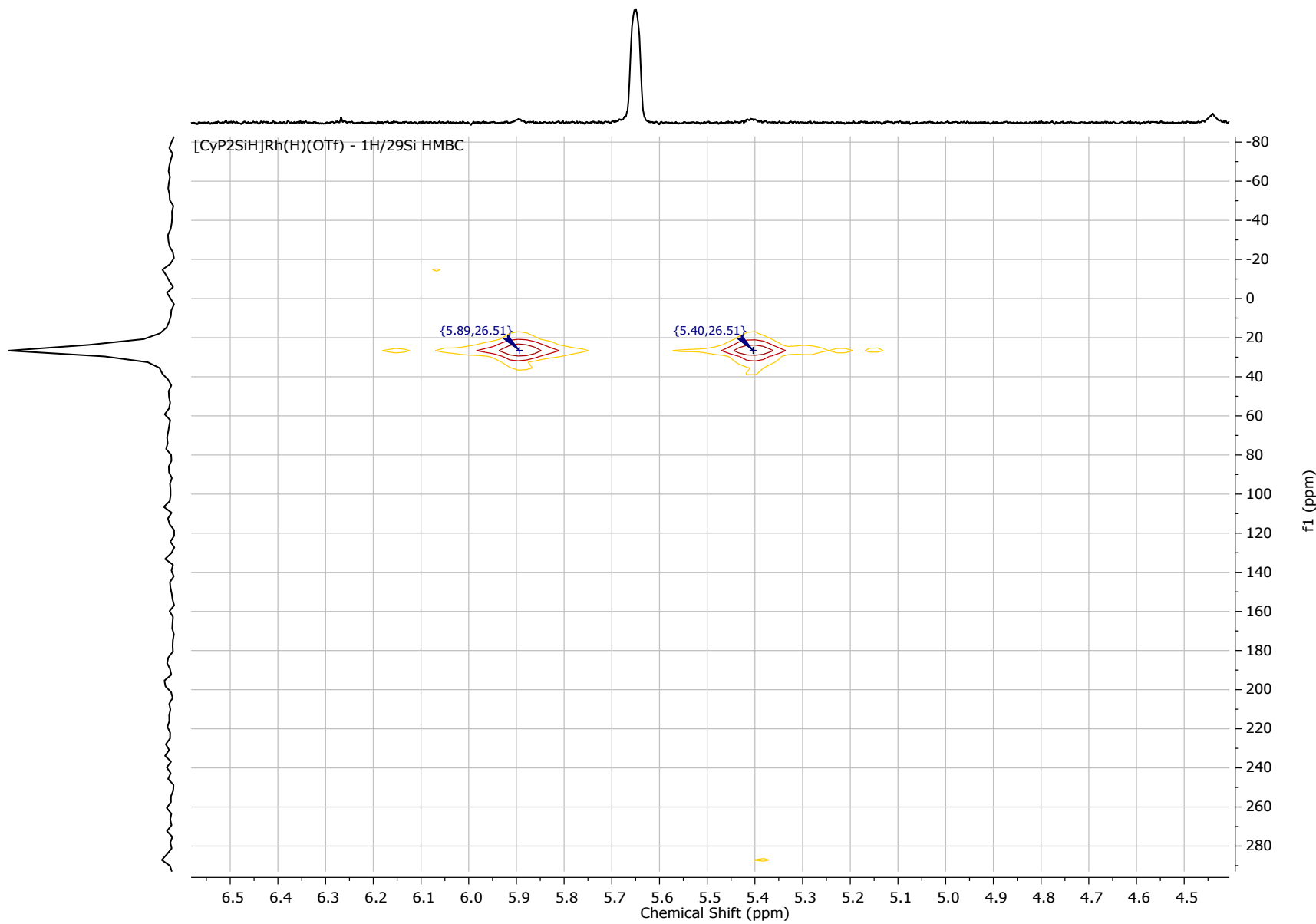


Figure S25. $^1\text{H}/^{29}\text{Si}$ HMQC NMR spectrum of $[\text{CyP}_2\text{Si}^{\text{H}}]\text{Rh}(\text{nbd})$ (Cy3-H) in C_6D_6

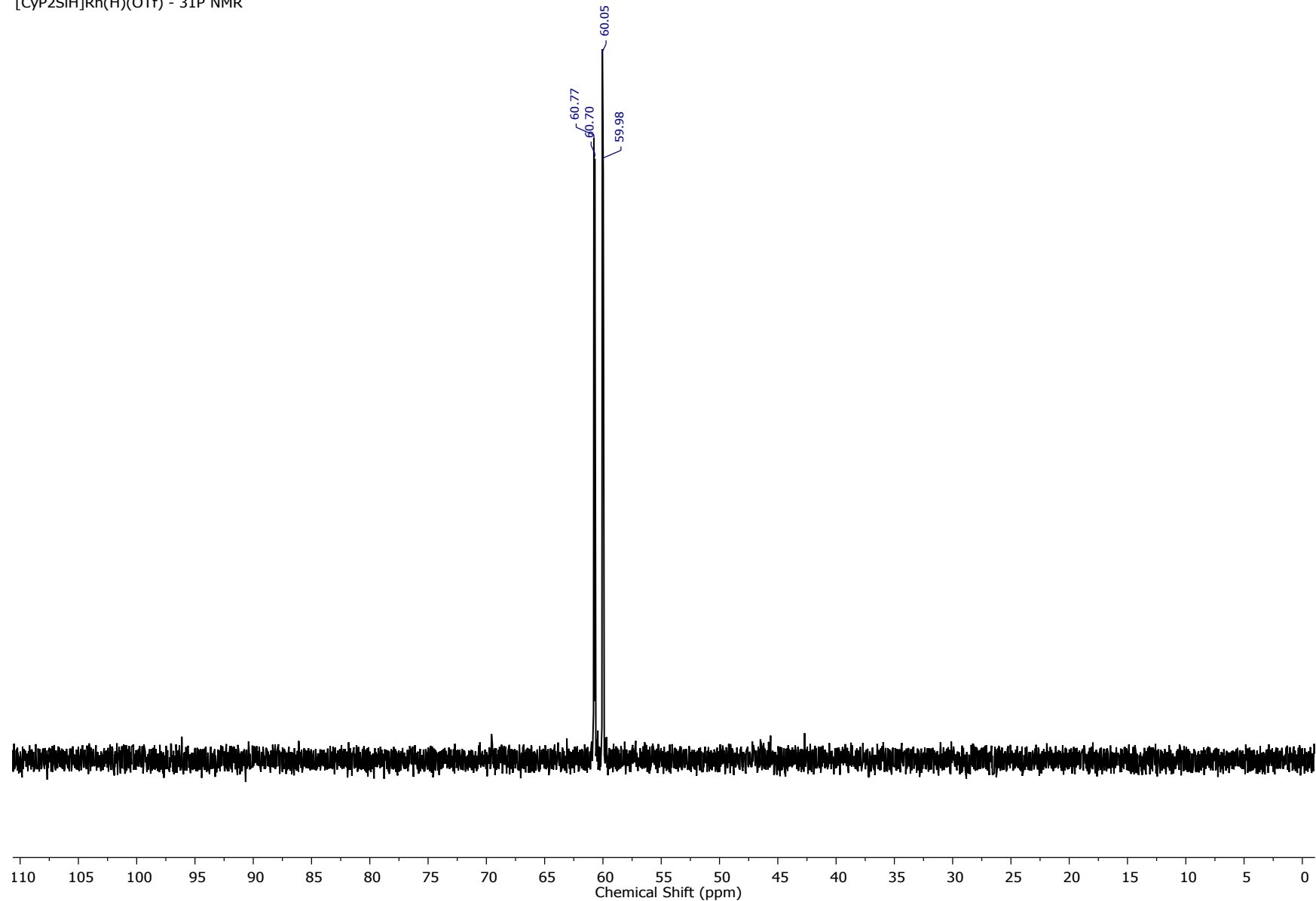


Figure S26. ³¹P NMR spectrum of ^[CyP₂SiH]Rh(nbd) (^{Cy3-H}) in C₆D₆

(CyP₂SiCH₃)Rh(H)(OTf) - ¹H NMR

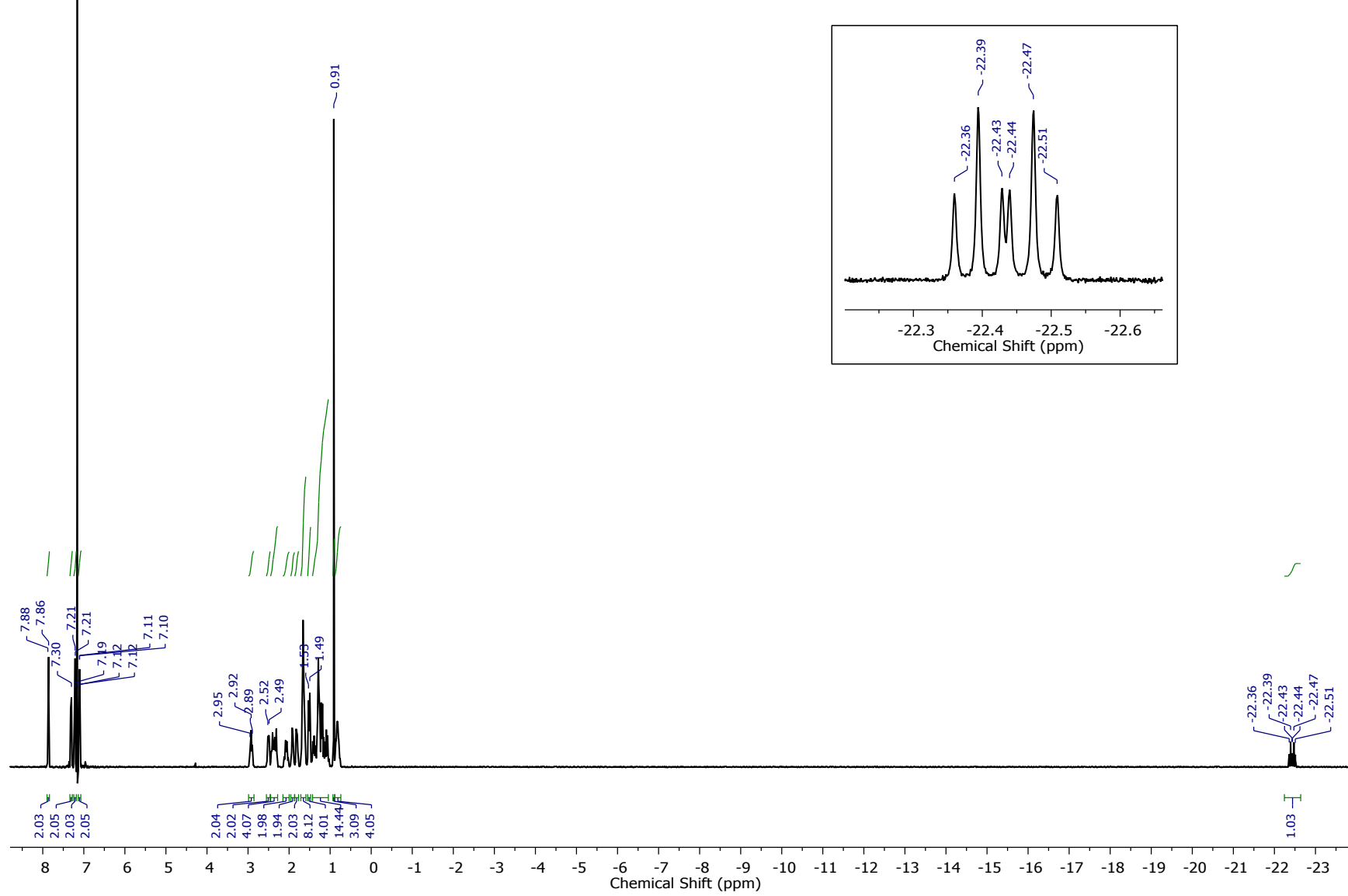


Figure S27. ¹H NMR spectrum of [CyP₂SiMe]Rh(H)(OTf) (^{Cy3-Me}) in C₆D₆

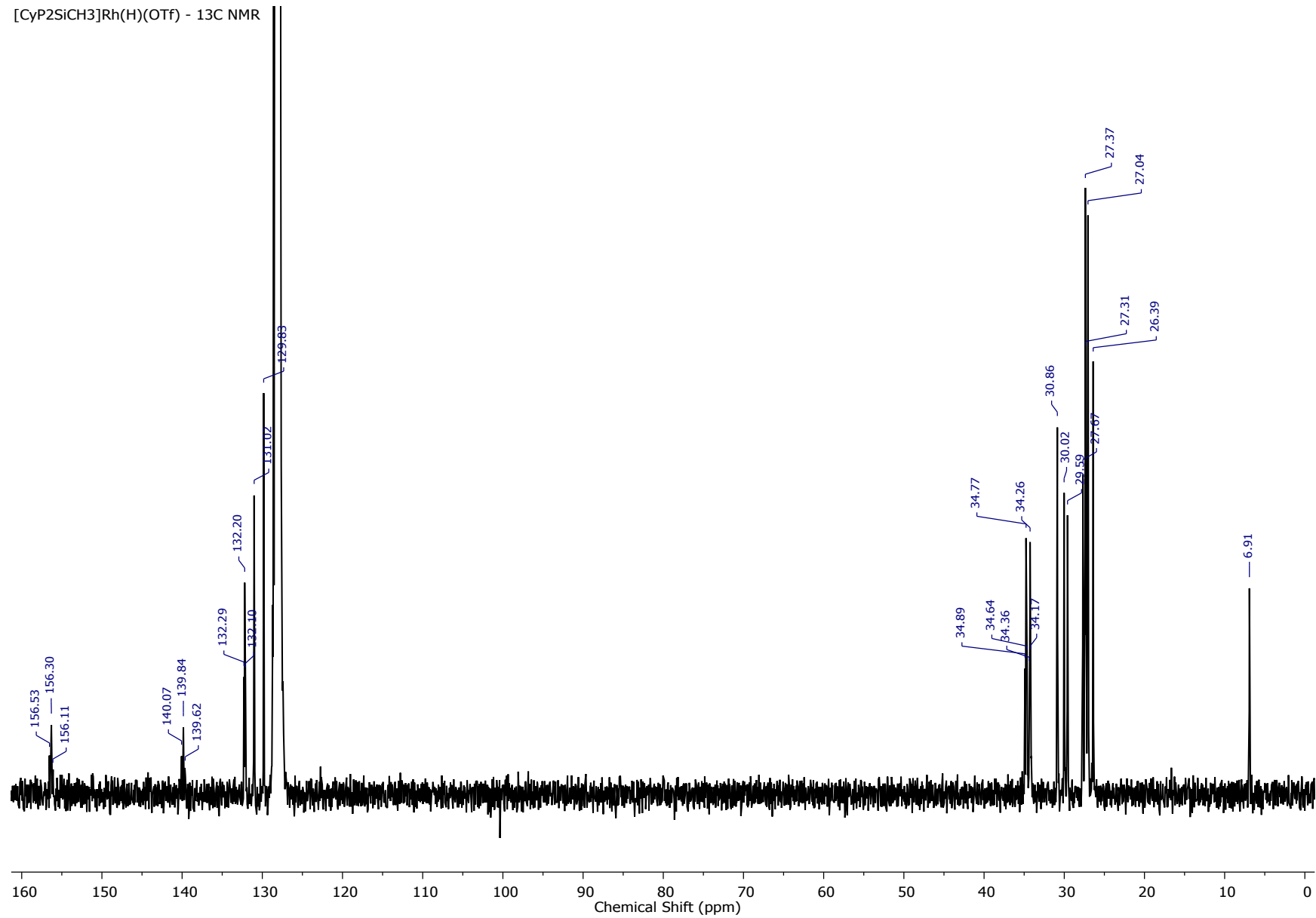


Figure S28. ¹³C NMR spectrum of [CyP₂SiMe]Rh(H)(OTf) (**Cy3-Me**) in C_6D_6

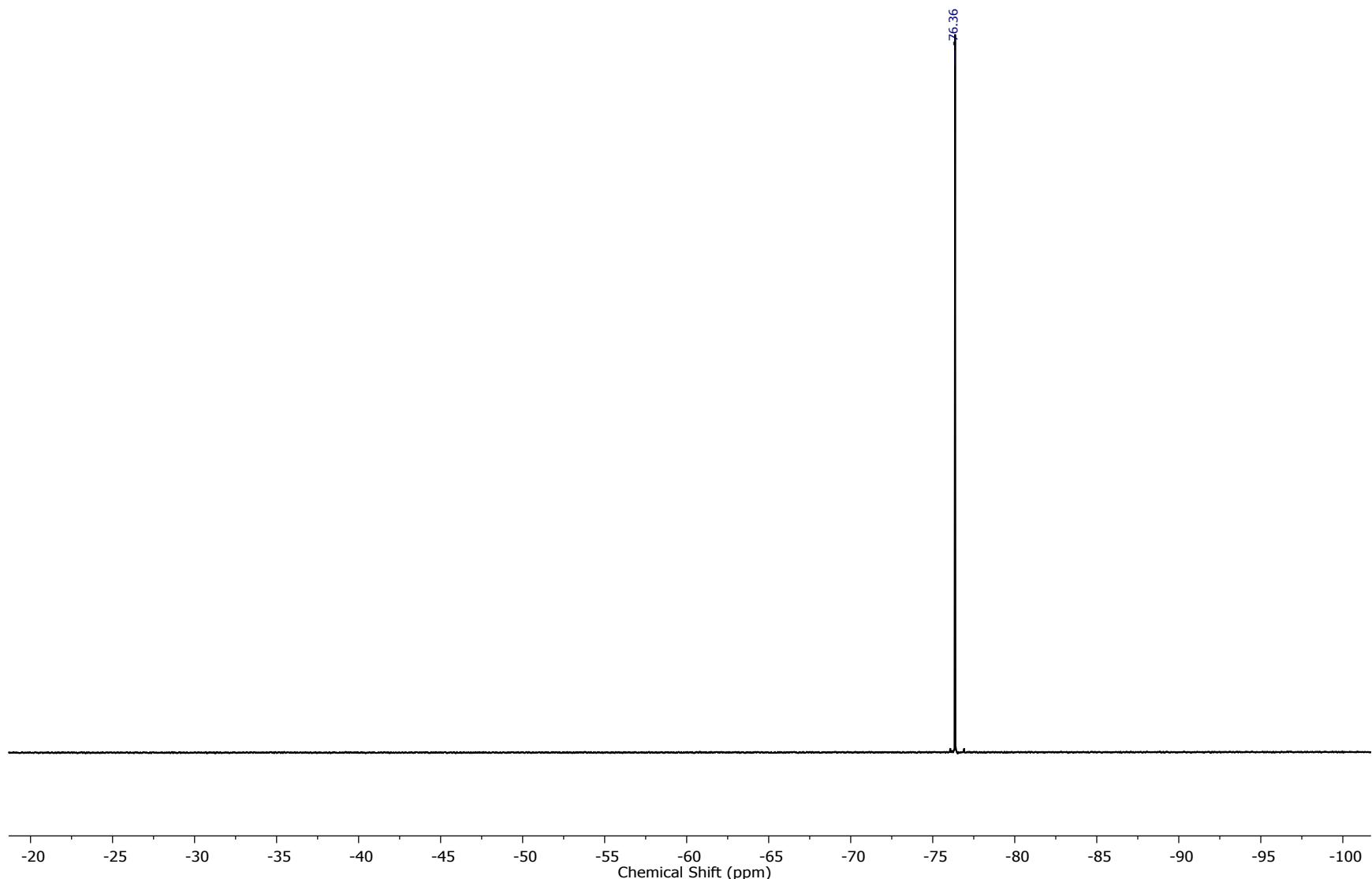


Figure S29. ¹⁹F NMR spectrum of [CyP₂SiMe]Rh(H)(OTf) (**Cy3-Me**) in C₆D₆

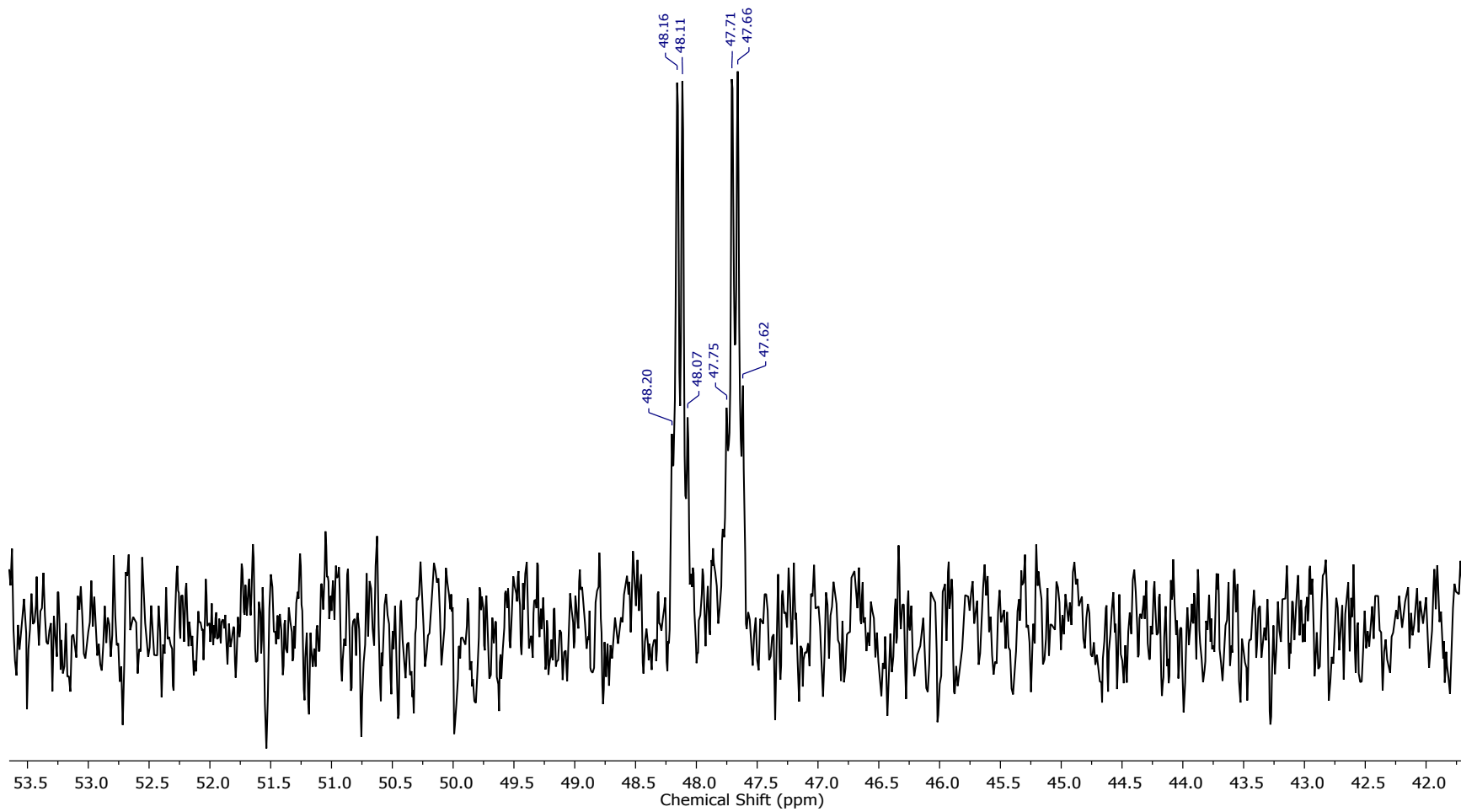


Figure S30. ²⁹Si NMR spectrum of [CyP₂SiⁱMe]Rh(H)(OTf) (**Cy3-Me**) in C₆D₆

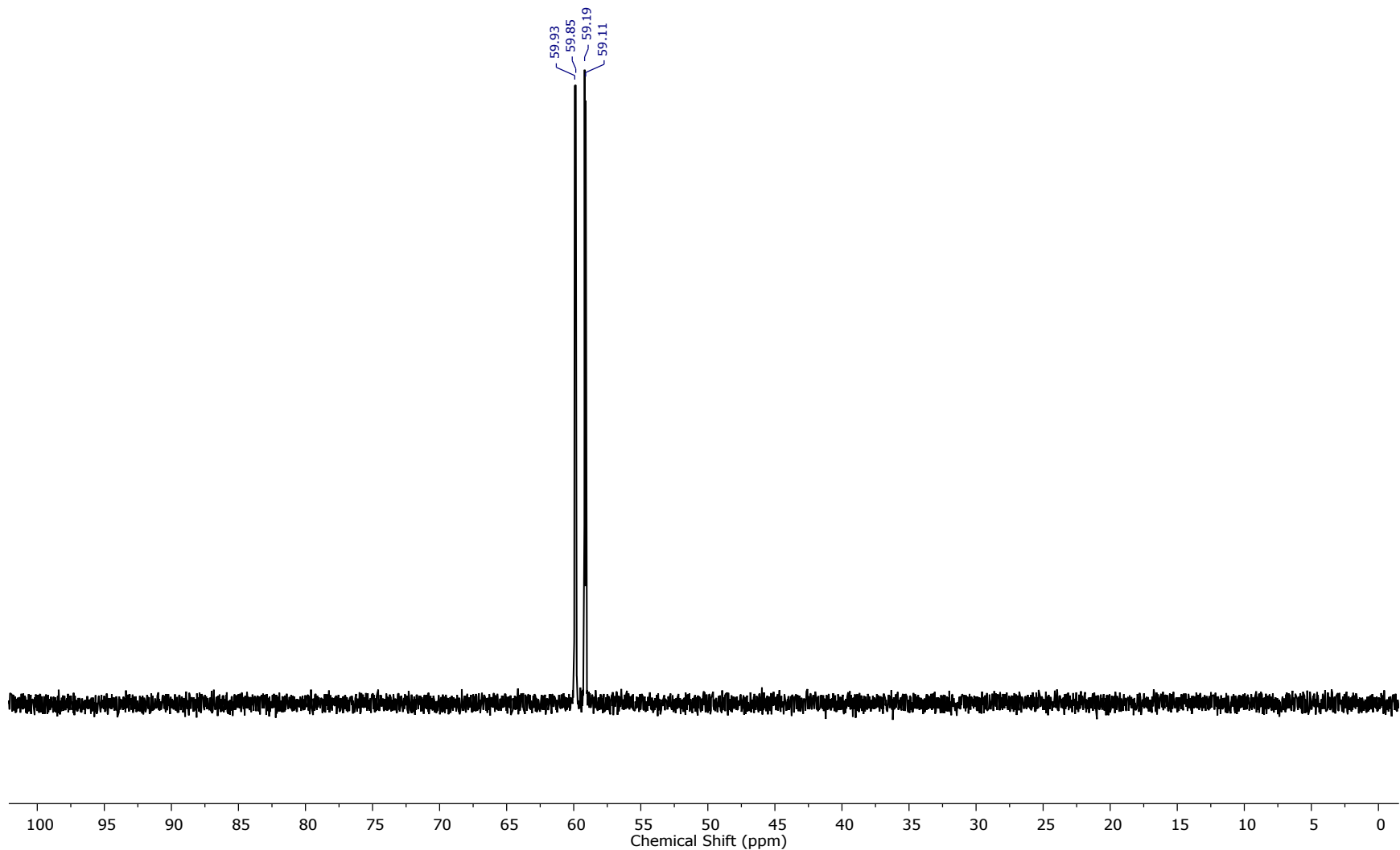


Figure S31. ³¹P NMR spectrum of [CyP₂SiMe]Rh(H)(OTf) (**Cy3-Me**) in C₆D₆

References

- 1 M. Murata and S. L. Buchwald, *Tetrahedron*, 2004, **60**, 7397-7403.
- 2 M. T. Whited, A. M. Deetz, J. W. Boerma, D. E. DeRosha and D. E. Janzen, *Organometallics*, 2014, **33**, 5070-5073.
- 3 D. F. MacLean, R. McDonald, M. J. Ferguson, A. J. Caddell and L. Turculet, *Chem. Commun.*, 2008, 5146-5148.
- 4 M. J. Frisch, G. W. Trucks, H. B. Schlegel, G. E. Scuseria, M. A. Robb, J. R. Cheeseman, G. Scalmani, V. Barone, B. Mennucci, G. A. Petersson, H. Nakatsuji, M. Caricato, X. Li, H. P. Hratchian, A. F. Izmaylov, J. Bloino, G. Zheng, J. L. Sonnenberg, M. Hada, M. Ehara, K. Toyota, R. Fukuda, J. Hasegawa, M. Ishida, T. Nakajima, Y. Honda, O. Kitao, H. Nakai, T. Vreven, J. A. Montgomery Jr., J. E. Peralta, F. Ogliaro, M. J. Bearpark, J. Heyd, E. N. Brothers, K. N. Kudin, V. N. Staroverov, R. Kobayashi, J. Normand, K. Raghavachari, A. P. Rendell, J. C. Burant, S. S. Iyengar, J. Tomasi, M. Cossi, N. Rega, N. J. Millam, M. Klene, J. E. Knox, J. B. Cross, V. Bakken, C. Adamo, J. Jaramillo, R. Gomperts, R. E. Stratmann, O. Yazyev, A. J. Austin, R. Cammi, C. Pomelli, J. W. Ochterski, R. L. Martin, K. Morokuma, V. G. Zakrzewski, G. A. Voth, P. Salvador, J. J. Dannenberg, S. Dapprich, A. D. Daniels, Ö. Farkas, J. B. Foresman, J. V. Ortiz, J. Cioslowski and D. J. Fox *Gaussian 09*, Gaussian, Inc.: Wallingford, CT, USA, 2009.
- 5 Y. Zhao and D. G. Truhlar, *Theor. Chem. Acc.*, 2008, **120**, 215-241.
- 6 (a) P. J. Hay and W. R. Wadt, *J. Chem. Phys.*, 1985, **82**, 270-283; (b) W. R. Wadt and P. J. Hay, *J. Chem. Phys.*, 1985, **82**, 284-298; (c) P. J. Hay and W. R. Wadt, *J. Chem. Phys.*, 1985, **82**, 299-310.
- 7 T. H. Dunning Jr. and P. J. Hay, in *Modern Theoretical Chemistry*, ed. H. F. Schaefer III, Plenum, New York, 1977, pp. 1-28.
- 8 G. Scalmani and M. J. Frisch, *J. Chem. Phys.*, 2010, **132**.
- 9 *CrystalClear*, Rigaku Americas and Rigaku: The Woodlands, TX, 2011.
- 10 O. V. Dolomanov, L. J. Bourhis, R. J. Gildea, J. A. K. Howard and H. Puschmann, *J. Appl. Cryst.*, 2009, **42**, 339-341.
- 11 L. J. Farrugia, *J. Appl. Cryst.*, 2012, **45**, 849-854.
- 12 *Persistence of Vision Raytracer (Version 3.6)*, Persistence of Vision Pty. Ltd.: 2004.
- 13 Spek, A. L. *J. Appl. Crystallogr.* 2003, **36**, 7–13.